JOURNAL OF VIROLOGY, Dec. 2011, p. 12410–12430 Vol. 85, No. 23
0022-538X/11/$12.00 doi:10.1128/JVI.05953-11

c-Cbl-Mediated Selective Virus-Receptor Translocations into Lipid Rafts Regulate Productive Kaposi's Sarcoma-Associated Herpesvirus Infection in Endothelial Cells[▽]

Sayan Chakraborty, Mohanan ValiyaVeettil, Sathish Sadagopan, Nitika Paudel, and Bala Chandran*

H. M. Bligh Cancer Research Laboratories, Department of Microbiology and Immunology, Chicago Medical School, Rosalind Franklin University of Medicine and Science, North Chicago, Illinois 60064

Received 10 August 2011/Accepted 12 September 2011

During target cell entry and infection, many enveloped and nonenveloped viruses utilize cell surface receptors that translocate into lipid rafts (LRs). However, the mechanism behind this translocation is not known. Kaposi's sarcoma-associated herpesvirus (KSHV) interacts with the human microvascular dermal endothelial (HMVEC-d) cell surface heparan sulfate (HS), integrins α3β1, αVβ3, and αVβ5, and the amino acid transporter x-CT protein and enters via c-Cbl-bleb-mediated macropinocytosis (Veettil et al., J. Virol. 82:12126-12144, 2008; Veettil et al., PLoS Pathog. 6:e1001238, 2010). Here we have demonstrated that very early during infection (1 min postinfection), c-Cbl induced the selective translocation of KSHV into the LR along with the α3β1, αVβ3, and x-CT receptors but not αVβ5. Activated c-Cbl localized with LRs at the junctional base of macropinocytic blebs. LR-translocated α3β1 and αVβ3 were monoubiquitinated, leading to productive macropinocytic entry, whereas non-LR-associated αVβ5 was polyubiquitinated, leading to clathrin entry that was targeted to lysosomes. c-Cbl knockdown blocked the macropinocytosis and receptor translocation and diverted KSHV to a clathrin-lysosomal noninfectious pathway. Similar results were also seen by LR disruption with MβCD. These studies provide the first evidence that c-Cbl regulates selective KSHV-α3β1, -αVβ3, and -x-CT receptor translocations into the LRs and differential ubiquitination of receptors which are critical determinants of the macropinocytic entry route and productive infection of KSHV. Our studies suggest that interventions targeting c-Cbl and LRs are potential avenues to block KSHV infection of endothelial cells.

Kaposi's sarcoma-associated herpesvirus (KSHV) is etiologically associated with Kaposi's sarcoma (KS), primary effusion lymphoma (PEL), and multicentric Castleman's disease (MCD) (6, 8, 10). Human B-cell lines from PEL, such as BCBL-1 and BC-3, carry multiple copies of the KSHV genome. The KSHV latency-associated LANA-1 (ORF73), vCyclin, vFLIP, Kaposin, and ORF10.5 (LANA-2) genes, as well as 12 microRNAs, are expressed in these cells. KSHV induced from these cells serves as the source of virus for various studies (10). In contrast to that of alpha- and betaherpesviruses, gamma-2 herpesvirus KSHV *in vitro* infection of target cells does not lead to the typical cascade of its immediate-early, early, and late gene expression and progeny virus formation. Instead, KSHV establishes latency, and the viral genome is lost during successive passages of the infected cells (7, 10, 21). Another novel feature of this *in vitro* latency in human microvascular dermal endothelial (HMVEC-d) and human foreskin fibroblast (HFF) cells is that as early as 2 h postinfection (p.i.), KSHV expresses concurrently its latent genes as well as a limited set of lytic cycle genes with antiapoptotic and immunomodulation functions, including the lytic cycle switch ORF50 (RTA) gene (21). While the expression of latent genes continues, nearly all lytic genes decline by 24 h p.i. (21).

Analysis of *in vitro* KSHV interaction with adherent target cells and quantitation of infection have been hampered by the absence of a lytic replication cycle and hence a plaque assay. Since *in vitro* KSHV infection results in the expression of latency-associated genes, we have devised various methods to assess the different phases of KSHV infection (7). For conceptual purposes, we earlier subdivided the early events of KSHV infection into six overlapping dynamic phases (7). Phase 1 involves the binding of viral envelope glycoproteins to cell surface receptors, overlapping with the induction of host cell signal pathways (phase 2). This is followed by virus entry (phase 3), movement of the viral capsid/tegument in the cytoplasm (phase 4), nuclear entry of the viral genome (phase 5), and the overlapping expression of viral genes (phase 6a) and host cell genes (phase 6b). To differentiate among and identify the phase(s) in which KSHV-induced host signal molecules play roles, we use an assortment of methods (7). Purified KSHV is quantitated by real-time DNA PCR for the single-copy gene ORF73 (7, 21, 38, 41, 45). Since the LANA-1 protein and messages are not incorporated in the virion particle, detection of LANA-1 in infected cells is due to *de novo* KSHV infection. Infection of cells with 10 KSHV DNA copies per cell results in the expression of ORF73 in >50% of infected cells as monitored by immunofluorescence assay (38).

A vivid mechanism as to how KSHV-recognized receptor interactions and induction of host signal molecules progress toward entry into target cells is essential for developing methods to control infection. The initial attachment to adherent

* Corresponding author. Mailing address: Department of Microbiology and Immunology, Chicago Medical School, Rosalind Franklin University of Medicine and Science, 3333 Green Bay Road, North Chicago, IL 60064. Phone: (847) 578-8822. Fax: (847) 578-3349. E-mail: bala.chandran@rosalindfranklin.edu.

▽ Published ahead of print on 21 September 2011.

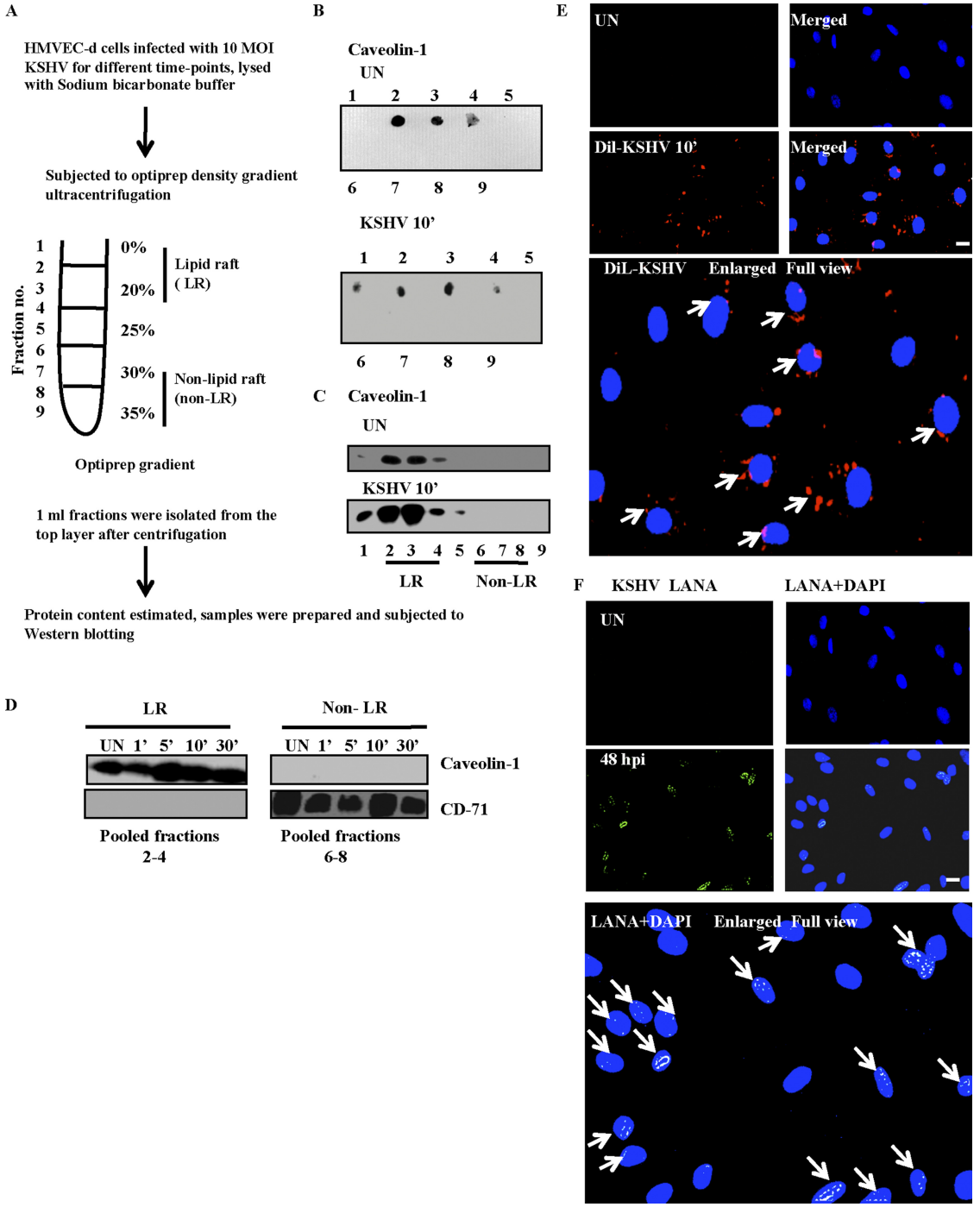

FIG. 1. Isolation and characterization of lipid rafts. (A) Flow chart of lipid raft (LR) extraction post-KSHV infection in serum-starved HMVEC-d cells. (B and C) Results with HMVEC-d cells infected with KSHV for 10 min. (B and C) Dot blot (B) or Western blot (C) for caveolin 1 (LR marker) in uninfected (UN) and KSHV-infected cells. (D) Caveolin 1 (LR marker) containing fractions 2 to 4 was pooled to form LR fractions, while CD-71 (NLR marker) containing fractions 6 to 8 was pooled to form non-LR fractions. Ten micrograms of protein from LR and non-LR fractions was subjected to Western blotting for caveolin 1 and CD-71. (E) HMVEC-d cells were mock or Dil-KSHV infected for 10 min. After washing, cells were fixed and observed by immunofluorescence microscopy. (F) HMVEC-d cells were mock or KSHV (10 DNA copies/cell) infected for 2 h, following which virus was washed away. Cells were cultured in complete medium for another 46 h. After washing, cells were fixed and processed for immunofluorescence assay using anti-LANA antibody. Ten different fields with at least 15 cells were counted to calculate the LANA and Dil-KSHV-positive cells. Representative deconvoluted images are shown. Arrows in the enlarged panel indicate infected cells. Scale bar, 10 μm.

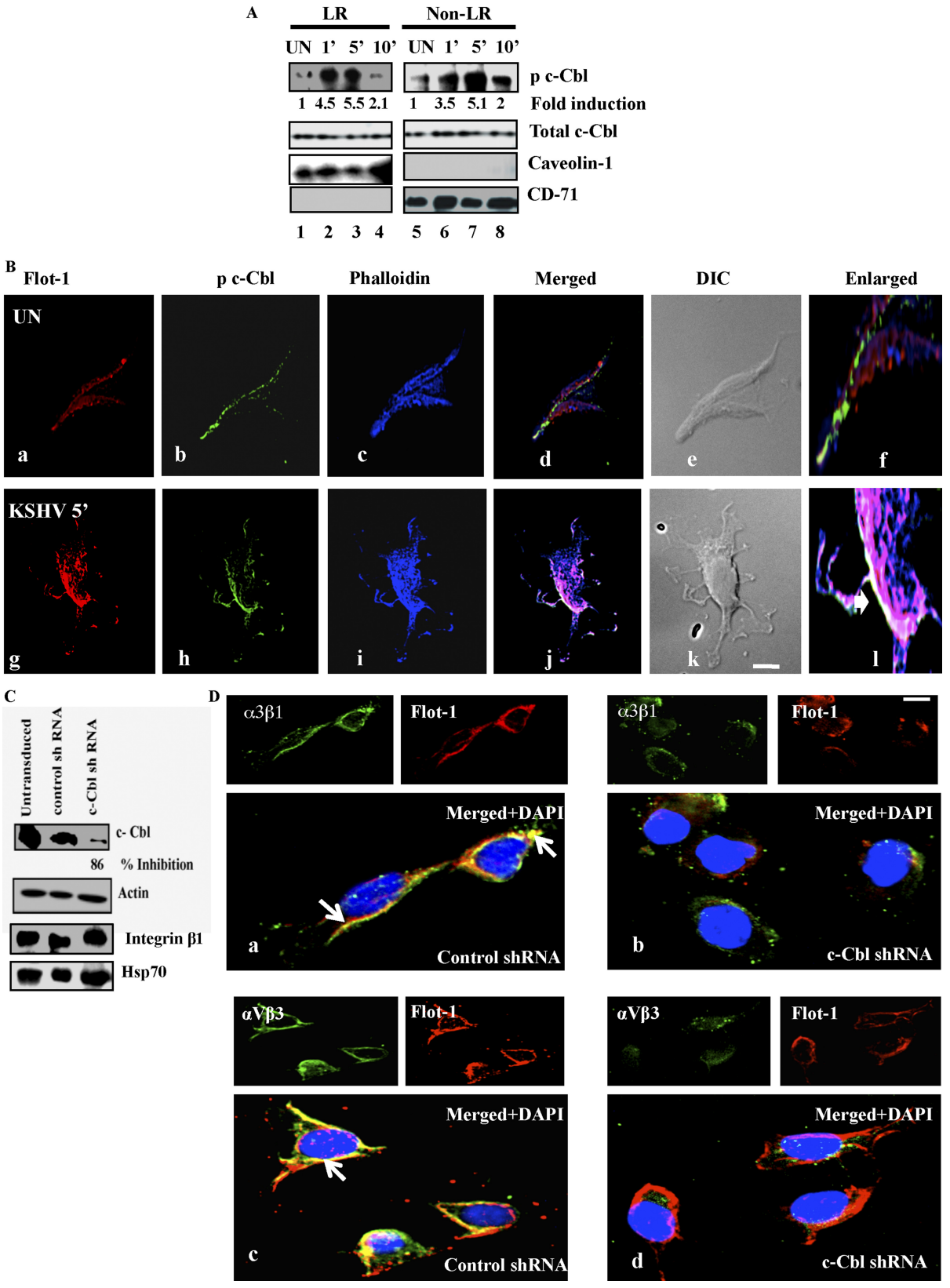

FIG. 2. Association of KSHV induced c-Cbl with lipid rafts, macropinocytic blebs and integrins (α3β1 and αVβ3). (A) Serum-starved (8 h) HMVEC-d cells were either mock or KSHV infected (10 DNA copies/cell) for the indicated time points. LR and NLR were isolated as described in the legend to Fig. 1A and Materials and Methods. Ten micrograms of protein was subjected to Western blotting for the indicated proteins. Student's *t* test was performed on the fold p-c-Cbl activation values between uninfected and KSHV-infected cell LR and non-LR fractions to obtain

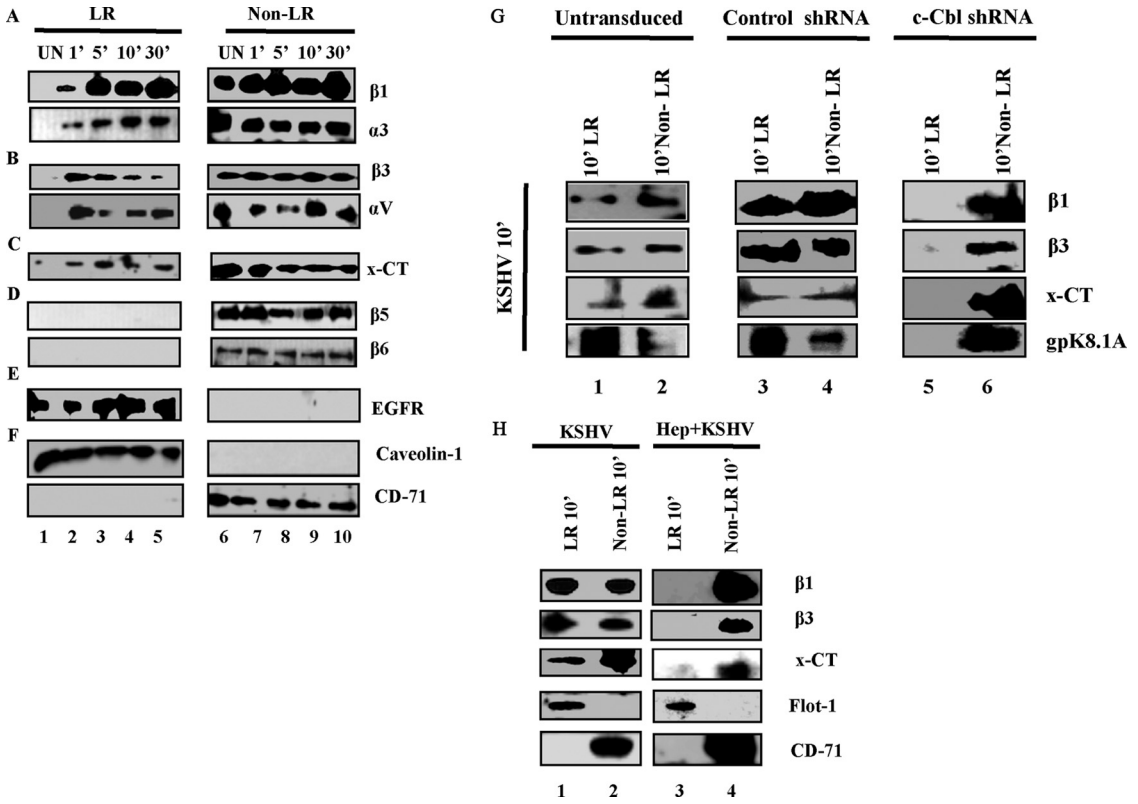

FIG. 3. c-Cbl-mediated selective translocation of integrins (α3β1 and αVβ3) and x-CT into lipid rafts early during KSHV infection. Serum-starved (8 h) HMVEC-d cells were either mock infected or KSHV infected (10 DNA copies/cell) for the indicated time points. LR and NLR fractions were isolated, and 10 μg protein was analyzed by Western blotting. (A) Integrins β1 and α3. (B) Integrins β3 and αV. (C) x-CT. (D) Integrins β5 and β6. (E) EGF receptor. (F) Caveolin 1 and CD-71 (markers of LR and non-LR, respectively). (G) Untransduced, control shRNA and c-Cbl shRNA lentivirus-transduced HMVEC-d cells were infected with KSHV for 10 min. LR and non-LR fractions were isolated and subjected to Western blot analysis for integrins β1 and β3, x-CT, and KSHV gpK8.1A. (H) Serum-starved HMVEC-d cells were infected with KSHV (lanes 1 and 2) or with KSHV preincubated with 50 μg heparin for 1 h at 37°C (lanes 3 and 4). LR and NLR were subjected to Western blotting for β1 integrin, β3 integrin, x-CT, flotillin 1 (LR marker), and CD-71 receptor (non-LR marker).

target cells is facilitated by KSHV envelope gB, gpK8.1A, gH, and ORF4 interaction with heparan sulfate (HS) molecules (1, 4, 16, 27, 49, 50). Pretreatment of KSHV with soluble heparin prevents binding of virus to the adherent target cells (7). KSHV subsequently interacts with the HMVEC-d cell integrins α3β1, αVβ3, and αVβ5 and the amino acid transporter x-CT protein (7). Heparin treatment also prevents KSHV interactions with α3β1, αVβ3, αVβ5, and x-CT molecules, suggesting that the initial contact with HS is essential for the subsequent interactions with other receptors (2, 19, 47). RGD peptides, soluble α3β1, αVβ3, and αVβ5 integrins, antibodies against α3β1, αVβ3, and αVβ5 integrins, and x-CT do not block KSHV binding to the adherent target cells; however, they inhibited KSHV entry and infection significantly, which suggested that inhibition occurs due to interference at a post-HS binding step.

Endocytosis is the predominant mode of KSHV entry into its adherent and nonadherent target cells (7). KSHV induces actin reorganization and enters HMVEC-d cells via macropinocytosis (37). Early during infection (1 to 30 min p.i.), KSHV forms a multimolecular complex with HS, integrins (α3β1, αVβ3, and αVβ5), and x-CT, with concurrent induction of

the *P* values. (B). Serum-starved HMVEC-d cells were either mock infected or KSHV infected (10 DNA copies/cell) for the indicated time points. Cells were stained with goat anti-flotillin-1 monoclonal antibody for 1 h at RT followed by Alexa 594 secondary antibody for 1 h at RT. Lipid raft labeled cells were further stained with mouse anti-phospho-c-Cbl pY 700 monoclonal antibody for 1 h at RT followed by Alexa 488 antimouse secondary antibody. Cells were costained with Alexa 405-conjugated phalloidin and observed under a deconvoluted immunofluorescence microscope equipped with differential interference contrast (DIC). Images were processed by Metamorph software. Arrowheads in the enlarged panel indicate colocalization. (C) Sixty to seventy percent confluent HMVEC-d cells in 6-well plates were either untransduced or transduced with control or c-Cbl shRNA lentiviruses and selected using puromycin. Untransduced, control shRNA- and c-Cbl shRNA cells were infected with KSHV (10 DNA copies/cell) for 5 min and analyzed by Western blotting for c-Cbl (specific shRNA target), actin, integrin β1, and Hsp70 (off-target molecules). The actin blot also represents an equal loading control. (D) Control and c-Cbl shRNA-transduced cells were infected with KSHV (10 DNA copies/cell) for 10 min and processed for immunofluorescence using an LR marker (Flot-1) and integrin α3β1 or αVβ3 antibodies. Representative confocal images are shown. Bottom panels are enlarged pictures merged with DAPI images. Arrows indicate colocalization. Scale bar, 10 μm.

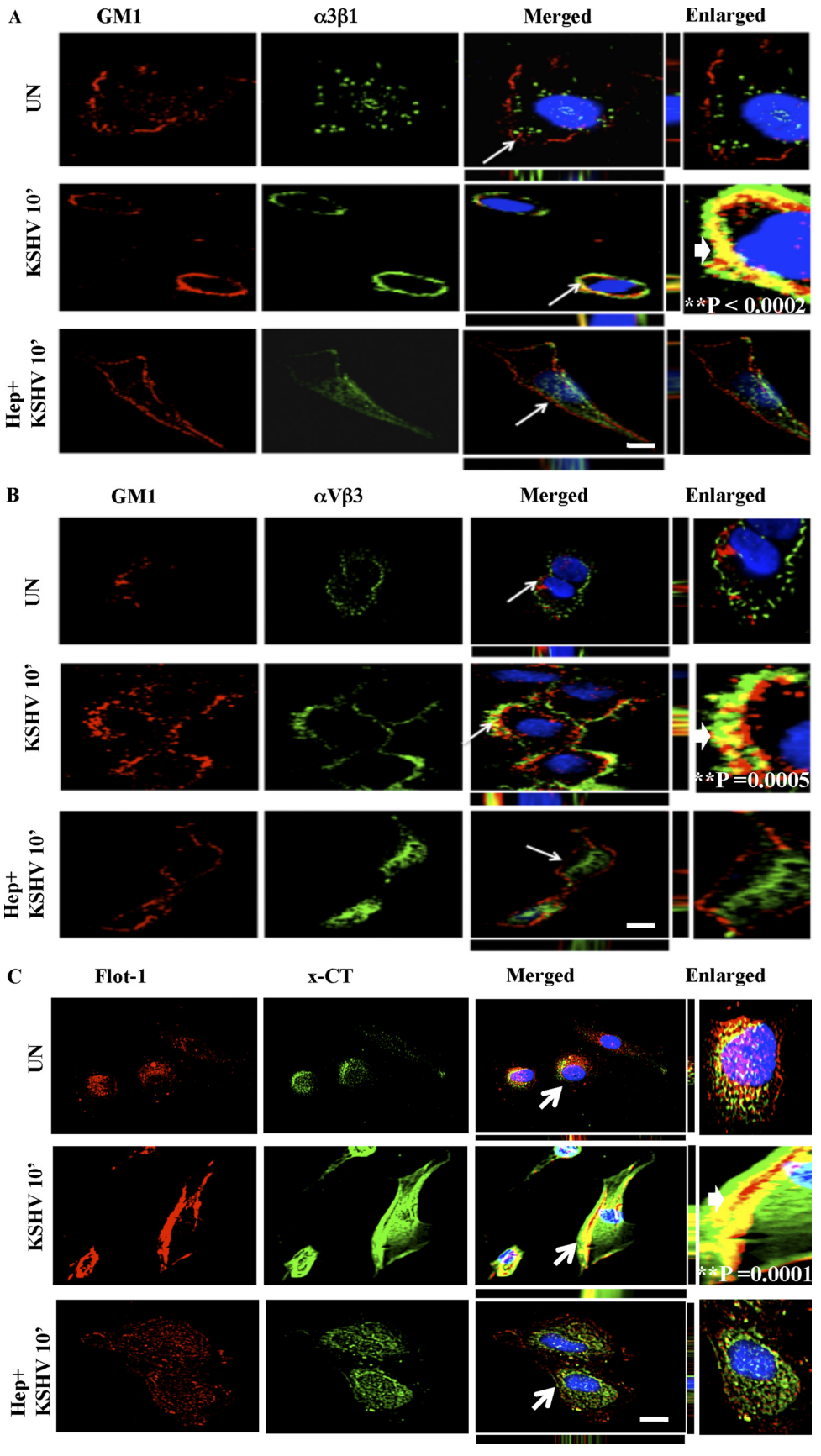
A
GM1
α3β1
Merged
Enlarged
UN
KSHV 10'
Hep+ KSHV 10'
**P < 0.0002
B
GM1
αVβ3
Merged
Enlarged
UN
KSHV 10'
Hep+ KSHV 10'
**P =0.0005
C
Flot-1
x-CT
Merged
Enlarged
UN
KSHV 10'
Hep+ KSHV 10'
**P =0.0001

signal cascades, such as FAK, Src, PI3-K and Rho-GTPases, that are essential for virion entry and trafficking in HMVEC-d cells (22, 29, 36, 48). Heparin treatment not only prevented binding of virus to the adherent target cells but also blocked the observed signal induction during 1 to 30 min p.i. Heparin-treated KSHV not only served as a specificity control for KSHV-induced signal induction and morphological changes but also clearly established the fact that the observed signal induction is due to KSHV virion particles and not due to any contaminating host factors, membranes, or LPS.

KSHV also induced membrane blebs and tyrosine phosphorylation of the adaptor protein c-Cbl as early as 1 min p.i., and its recruitment to the sites of bleb formation was required for blebbing and macropinocytosis in HMVEC-d cells (45). Pretreatment of KSHV with soluble heparin not only prevented macropinocytosis and entry of virus but also reduced the phosphorylation of c-Cbl phosphorylation. c-Cbl small-hairpin RNA (shRNA) decreased KSHV ORF73 and ORF50 gene expression by >90%, which was due to a block in KSHV macropinocytosis and entry but not binding to the target cells (45).

Lipid rafts (LRs), the detergent-resistant microdomains in the exoplasmic leaflet of plasma membranes, are made up of cholesterol and sphingolipids (sphingomyelin and glycosphingolipids) and play roles in clustering receptors and signal molecules (42). The interaction between different receptors on the plasma membrane is considered an important mechanism for coordination of signaling pathways, often manifested by dynamic membrane alterations (12). LRs are utilized for entry by many enveloped and nonenveloped viruses. Echo- and coxsackieviruses utilize LRs for endocytosis and entry, respectively (31, 32). HIV-1 and human cytomegalovirus (HCMV) interact with LR-associated molecules and non-LR (NLR)-associated molecules and pull the NLR-associated secondary receptor into LRs (5, 35, 51). During infection of $CD4^+$ T cells, HIV-1 gp120 interacts with LR-associated CD4 molecules and subsequently with NLR-associated chemokine receptor CXCR4, which results in the translocation of CXCR4 into LR, and these raft-colocalized receptors are directly involved in virus entry (5, 35). Similarly, HCMV interacts with human embryonic lung fibroblast (HEL) LR-associated epidermal growth factor receptor (EGFR)- and NLR-associated αVβ3 integrin, which subsequently associates with LR (51). However, the mechanism and molecular partners regulating the translocation of NLR-associated molecules into LR remain unknown.

Our previous studies revealed that LRs are essential for KSHV infection of HMVEC-d cells. Pretreatment of HMVEC-d cells with LR-disrupting drugs (MβCD or nystatin), though it did not affect virus binding and entry, inhibited KSHV-induced phosphatidylinositol 3-kinase (PI3-K) and RhoA-GTPase molecules, association of viral capsid with microtubules, and nuclear entry of viral DNA and viral gene expression (36). However, the functional link between a KSHV entry receptor(s), c-Cbl, and LRs, as well as whether this link facilitates virus entry, was unknown and was examined here.

KSHV infection induced a c-Cbl-dependent selective translocation of α3β1, αVβ3, and x-CT molecules into the LR, while αVβ5 remained in the NLR region of the membranes. KSHV-activated c-Cbl's ability to monoubiquitinate receptors was potentially driving the translocation of KSHV and the associated receptors into LRs, resulting in a productive infection, while NLR-partitioned αVβ5 was polyubiquitinated and targeted to lysosomes. c-Cbl knockdown resulted in the abrogation of the selective virus-receptor translocation or macropinocytosis and diverted KSHV toward clathrin-mediated lysosomal targeting, thus inhibiting infection. Our studies shed light on a unique role of c-Cbl as a modulator of endocytic pathways regulating the fate of KSHV.

MATERIALS AND METHODS

Cells and virus. HMVEC-d cells (CC-2543; Clonetics, Walkersville, MD) were grown in endothelial cell basal medium 2 (EBM2; Clonetics). Induction of the KSHV lytic cycle in BCBL-1 cells, supernatant collection, and virus purification procedures were described previously (2). KSHV DNA was extracted from the virus, and the copies were quantitated by real-time DNA PCR using primers amplifying the KSHV ORF73 gene as described previously (21). The same batch of purified KSHV was used for all experiments.

Dil-labeled KSHV. The lipophilic carbocyanine DiI-1,1′-dioctadecyl-3,3,3′,3′-tetramethylindocarbocyanine perchlorate ($DiIC_{18}3$) was used to label KSHV particles as per methods described previously (23). Briefly, 200 μl of 1-mg/ml purified KSHV in TNE–30% sucrose buffer (TNE buffer is 0.01 M Tris-HCl, pH 7.4, 0.15 M NaCl, and 0.05% EDTA) was incubated with 25 mM Dil in dimethyl sulfoxide (DMSO) for 2 h at room temperature (RT) with gentle mixing. The unbound dye was removed by a step sucrose gradient (10%, 30%, and 55% [wt/vol] sucrose in TNE buffer). Dil-labeled KSHV was layered on top of the 10% sucrose cushion and centrifuged at 55,000 × *g* for 90 min at 4°C. The labeled virus collected from the top of the 55% sucrose gradient was filtered (22 μm pore size) and used.

Generation of HMVEC-d cells expressing c-Cbl shRNA. A pool of lentivirus shRNA specific for human c-Cbl and nonspecific control shRNA were purchased from Santa Cruz Biotechnology Inc., Santa Cruz, CA. HMVEC-d cells were transduced with control lentivirus shRNA or c-Cbl lentivirus shRNA according to the manufacturer's instructions and selected by puromycin hydrochloride (10 μg/ml).

Antibodies and reagents. Rabbit anti-integrin β1, β3, and anti-c-Cbl antibodies were from Cell Signaling Technology, Danvers, MA. Mouse anti-integrin α3β1, β5, α3, αV, β6, c-Cbl, and FK-1 antipolyubiquitin antibodies were from

FIG. 4. Colocalization of integrins (α3β1 and αVβ3) and x-CT with lipid raft markers during KSHV infection of HMVEC-d cells**.** Serum-starved (8 h) HMVEC-d cells were either left uninfected or infected for 10 min with KSHV (10 DNA copies/cell) or KSHV preincubated with 50 μg heparin for 1 h at 37°C, washed, and processed for immunofluorescence assay. Cells were stained for GM1 by incubating them with Alexa 594-conjugated CTxB for 45 min at 4°C, washed three times with chilled HBSS, and incubated with anti-CTB for 45 min at 4°C. These lipid raft labeled cells were costained with mouse anti-integrin α3β1 antibody for 1 h at RT followed by Alexa 488 anti-mouse antibody for 1 h at RT (A); mouse anti-αVβ3 integrin monoclonal antibody for 1 h at RT followed by Alexa 488 anti-mouse antibody for 1 h at RT (B); or anti-flotillin-1 (LR) and x-CT peptide (66-77) antibodies followed by Alexa 594 anti-goat and Alexa 488 anti-rabbit antibodies, respectively (C). They were visualized by a confocal immunofluorescence microscope and costained with DAPI. Arrows indicate the area of the cell enlarged in the rightmost panel. Block arrows in the enlarged panels indicate colocalization. Scale bar, 10 μm. *P* values were calculated between the percentage of uninfected versus KSHV-infected cells demonstrating colocalization of GM1 (LR) and α3β1, αVβ3, and x-CT using a Student *t* test. A minimum of 10 cells/field were chosen for colocalization analysis.

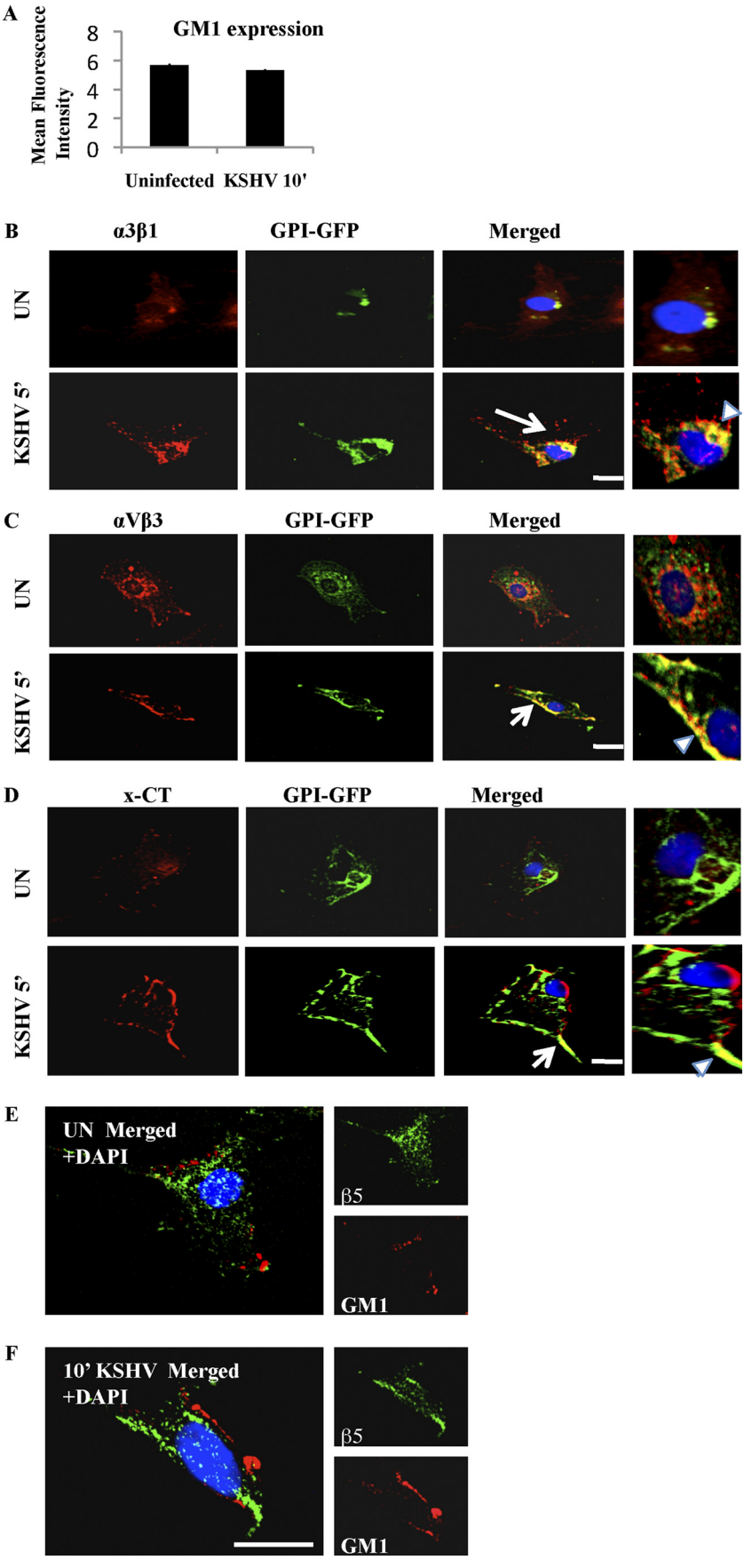
A
GM1 expression
Mean Fluorescence Intensity
8
6
4
2
0
Uninfected
KSHV 10'
B
α3β1
GPI-GFP
Merged
UN
KSHV 5'
C
αVβ3
GPI-GFP
Merged
UN
KSHV 5'
D
x-CT
GPI-GFP
Merged
UN
KSHV 5'
E
UN Merged +DAPI
β5
GM1
F
10' KSHV Merged +DAPI
β5
GM1

Chemicon International, Temecula, CA. Mouse monoclonal anti-EGFR and anti-ubiquitin P4D1 antibodies were from Santa Cruz Biotechnology. Mouse anti-c-Cbl and anti-phospho-c-Cbl pY700 (phosphotyrosine) were from BD Biosciences, San Diego, CA. Rabbit anti-caveolin-1 antibody, anti-cholera toxin B (CTxB) antibody, CTxB-Alexa 594 conjugate, 4′,6-diamidino-2-phenylindole (DAPI), Alexa 488-conjugated LysoTracker, rhodamine-conjugated dextran or transferrin, Alexa 594 or 488 anti-rabbit, DiI (1,1′-dioctadecyl 3,3,3′,3′-tetramethylindocarbocyanine perchlorate), antimouse, and antigoat secondary antibodies were from Molecular Probes, Invitrogen. Goat monoclonal anti-flotillin-1 (anti-Flot-1) antibody was from Abcam, Boston, MA. Protein G Sepharose CL-4B was from Amersham Pharmacia Biotech, Piscataway, NJ. Anti-goat, anti-rabbit, and anti-mouse antibodies linked to horseradish peroxidase were from KPL Inc., Gaithersburg, MD. Heparin and MG132 were from Sigma, St. Louis, MO. The CD-71 hybridoma cell line was from American Type Culture Collection (ATCC), Manassas, VA. CD-71 monoclonal antibody (MAb) secreted in culture medium was purified by protein A-Sepharose affinity chromatography. Rabbit anti-x-CT peptide P66-77 (extracellular domain) antibody, mouse monoclonal anti-KSHV gpK8.1A (4A4) antibody, and rabbit anti-gB (UK-218) and anti-LANA antibodies were raised in our laboratory (38, 47, 50, 53).

Lipid raft extraction and characterization. Lipid raft extraction was performed as per the manufacturer's protocol for the caveola/raft isolation kit (Sigma) based on nondetergent density gradient extraction of lipid rafts (43). Briefly, uninfected and KSHV-infected HMVEC-d cells were lysed in 0.5 M sodium bicarbonate buffer (500 mM sodium carbonate [pH 11.0], 2 mM EDTA, 1 mM NaF, 1 mM orthovanadate, and Sigma protease cocktail inhibitor) for 15 min at 4°C. Cell lysates transferred onto precooled microcentrifuge tubes were homogenized using a Dounce homogenizer (10 strokes) and sonicated for 10 s. A discontinuous density gradient made of 5 layers of OptiPrep with different concentrations (Fig. 1A) was prepared. Two ml of gradient layer (35% OptiPrep) was placed at the bottom of the precooled ultracentrifuge tube. Each OptiPrep layer was placed over the other using a Pasteur pipette. The tubes were ultracentrifuged at 45,000 rpm for 4 h using a Beckman SWI-55 rotor. One-milliliter fractions were collected from the top of the centrifuge tube and pooled. Lipid raft-containing fractions were characterized by the presence of caveolin 1, and non-lipid rafts were confirmed by the presence of CD-71 (26).

Immunoprecipitation. LR and NLR fractions were isolated as described previously. Two hundred micrograms of cell lysates were incubated for 2 h with immunoprecipitating antibody at 4°C, and the resulting immune complexes were captured by protein G-Sepharose, washed 3 times using sodium bicarbonate buffer, and analyzed by Western blotting using specific detection antibodies.

Dot blot analysis. Two microliters of collected fractions were absorbed onto a nitrocellulose membrane soaked in 1× phosphate-buffered saline (PBS), blocked in 5% skimmed-milk solution for 1 h at RT, and incubated with anti-caveolin-1 antibody for 1 h at RT, followed by 3 subsequent washes with 1× PBS. The blot was incubated with species-specific horseradish peroxidase (HRP)-conjugated secondary antibody. Immunoreactive dots were visualized by enhanced chemiluminescence (Pierce, Rockford, IL) according to the manufacturer's instructions.

Western blotting. Cells were lysed in a sodium bicarbonate buffer (pH 11) and protease inhibitor mixture and incubated on a rocker at 4°C for 15 min. Lysates were normalized to equal amounts of protein, separated by 10% SDS-PAGE, transferred to nitrocellulose, and probed with the indicated primary antibodies. Detection was by incubation with species-specific HRP-conjugated secondary antibodies. Immunoreactive bands were visualized by enhanced chemiluminescence. The bands were scanned and quantitated using the FluorChemFC2 and Alpha-Imager (Alpha Innotech Corporation, San Leonardo, CA) imaging systems.

Immunofluorescence microscopy. HMVEC-d cells seeded on 8-well chamber slides (Nalge Nunc International, Naperville, IL) were used. Infected and uninfected cells were fixed with 4% paraformaldehyde for 15 min, permeabilized with 0.2% Triton X-100, and blocked with Image-iTFX signal enhancer (Invitrogen). The cells were reacted with primary antibodies followed by fluorescent dye-conjugated secondary antibodies. For colocalization with dextran and transferrin, cells were incubated with the fluid-phase marker dextran Texas Red (40 kDa, 0.5 mg/ml; Invitrogen) or Alexa 594 transferrin (35 $\mu g\ ml^{-1}$; Invitrogen) at 37°C in the presence of KSHV, followed by immunostaining with the appropriate antibodies. Cells were imaged with a Nikon fluorescence microscope equipped with a Metamorph digital imaging system.

For confocal analysis, the Olympus 300 microscope was used for imaging, and analysis was performed using the Fluoview software program (Olympus, Melville, NY). All experiments were performed at least three times.

Plasmids and transfection. HMVEC-d cells were grown in endothelial cell medium. Glycosylphosphatidylinositol (GPI)-green fluorescent protein (GFP)-tagged plasmids were generously provided by Kai Simons, Max-Planck-Institute of Molecular Cell Biology and Genetics, Dresden, Germany. Transfection was performed using 5 μg of plasmid DNA, Lipofectamine 2000 (Invitrogen), and Opti-MEM medium (Invitrogen) according to the manufacturer's instructions. GFP expression was monitored 18 to 24 h posttransfection. After transfection, cells were cultured for 48 h. Cells were serum starved and processed for immunofluorescence.

GM1 surface expression measurement. HMVEC-d cells were either mock or KSHV infected (10 DNA copies/cell), washed in Hanks balanced salt solution (HBSS), trypsinized, blocked, and stained with CTxB conjugate for 45 min at 4°C, followed by anti-CTxB secondary antibody. Cells were then fixed in Cytofix solution and processed for flow cytometry.

RESULTS

Isolation and characterization of lipid rafts of uninfected and KSHV-infected endothelial (HMVEC-d) cells. LRs from HMVEC-d cells infected with KSHV for different time points were separated from non-lipid rafts (NLRs) (Fig. 1A) by a previously described method (26, 43). This method isolates only the plasma membrane LRs and not the internal endosomal membranes, which require a step gradient centrifugation procedure (13). When the purity of isolated fractions was assessed, as reported before (33), the LR resident caveolin-1 (22-kDa) protein was detected in fractions 1 to 4, indicating that these were low-density LR fractions. In contrast, fractions 6 to 8 were negative for caveolin 1, indicating that they were high-density NLR fractions (Fig. 1B). Western blot analysis for caveolin 1 further confirmed fractions 1 to 5 as LR and fractions 6 to 9 as NLR (Fig. 1C). The enrichment of caveolin 1 in the LR fractions was observed in both uninfected and KSHV-infected cells (Fig. 1B and C). This clearly demonstrated that KSHV infection does not alter the low-density distribution of bona fide raft-associated proteins and the biochemical characteristics of LR remained unchanged with KSHV infection. Hence, we considered pooled fractions 2 to 4 as LR fractions

FIG. 5. GM1 expression and KSHV receptor association with LR markers. (A) HMVEC-d cells were either mock or KSHV infected (10 DNA copies/cell), washed in HBSS, trypsinized, blocked, and stained with CTxB conjugate for 45 min at 4°C followed by anti-CTxB secondary antibody. Cells were then fixed in Cytofix solution and processed for flow cytometry. (B to D) HMVEC-d cells were transfected with 5 μg GPI-GFP using Lipofectamine 2000. Forty-eight hours posttransfection, cells were either mock infected or KSHV infected (10 DNA copies/cell) for the indicated time points, fixed in 2% paraformaldehyde for 15 min at RT, and tested with anti-integrin α3β1, integrin αVβ3, and x-CT antibodies and respective secondary antibodies. Arrows in the merged panel indicate the area of the cell enlarged. Arrowheads in enlarged panels indicate colocalization. Scale bar, 10 μm. (E and F) Serum-starved (8 h) HMVEC-d cells were either left uninfected or infected for 10 min with KSHV (10 DNA copies per cell), washed three times with HBSS, fixed with 4% paraformaldehyde for 15 min at RT, and permeabilized with 0.2% Triton X-100 for 5 min at RT. Cells were blocked with signal enhancer for 20 min and stained for GM1 by incubating with Alexa 594-conjugated CTxB for 45 min at 4°C, washed three times with chilled HBSS, and incubated with anti-CTB for 45 min at 4°C. These lipid raft labeled cells were costained with mouse anti-integrin αVβ5 monoclonal antibody for 1 h at RT followed by Alexa 488 anti-mouse antibody for 1 h at RT. Scale bar, 10 μm.

and pooled fractions 6 to 8 as NLR fractions. Caveolin 1 was associated only with LR fractions and not with NLR fractions (Fig. 1D). NLR fractions were enriched with transferrin receptor (CD-71; 80-kDa), a classical NLR marker (17), which also confirmed our designation of pooled fractions 6 to 8 as NLR (Fig. 1D).

c-Cbl is recruited to lipid rafts at the junctional base of macropinocytic blebs early during KSHV infection of HMVEC-d cells. To prove that infection of cells with 10 KSHV DNA copies/cell can result in uniform infection and to determine the percentage of infected cells, we used lipophilic Dil dye-labeled KSHV. At 10 min p.i., we observed >60 to 70% Dil-KSHV in the infected cells, indicated by peripheral dot-like virion particle staining (Fig. 1E). At 48 h p.i., characteristic punctate nuclear LANA-1 dots were observed in about 61% of cells (Fig. 1F).

Western blot analysis revealed the association of phospho-c-Cbl (p-c-Cbl) with LR and NLR fractions early during KSHV infection (Fig. 2A). Although p-c-Cbl was LR associated in uninfected cells, as early as 1 min p.i. the infected-cell LR-associated p-c-Cbl increased to a significant level ($P < 0.009$) at about 4.5-fold induction, maximized to about 5.5-fold by 5 min p.i. and reduced by 2.1-fold at 10 min p.i. (Fig. 2A, LR fractions). A similar pattern of significant c-Cbl activation ($P < 0.008$) was also observed in NLR fractions, with about 3.5-, 5.1-, and 2-fold induction at 1, 5, and 10 min p.i., respectively (Fig. 2A). Total c-Cbl distribution was equal in both LR and NLR fractions. Caveolin-1 and CD-71 levels characterized the purity of LR and NLR fractions, respectively (Fig. 2A).

Our previous studies have elucidated the recruitment of c-Cbl-actin dynamics during macropinocytosis of KSHV (45). We next investigated whether LR-associated c-Cbl was located in proximity to membrane blebs induced by KSHV. Compared to uninfected cells, KSHV-infected cells revealed plasma-membrane protrusions in the form of blebs (Fig. 2B, panels e and k). Interestingly, p c-Cbl, LR, and actin colocalized at the junctional base of blebs in KSHV-infected cells at 5 min p.i. (Fig. 2B, panel l, white region). This suggested that LR-associated c-Cbl was involved in macropinocytosis during KSHV infection in the infected cells.

c-Cbl mediates selective translocation of KSHV receptors into lipid rafts early during KSHV infection of HMVEC-d cells. Since we observed raft-associated c-Cbl in proximity to macropinocytic blebs during early infection, we asked whether c-Cbl played any role in the recruitment of a KSHV-bound receptor(s) into LR. To test this, we used c-Cbl lentivirus encoding shRNAs to knock down c-Cbl activity in HMVEC-d cells. The c-Cbl-specific shRNA inhibited 86% of c-Cbl expression as detected by Western blotting with an antibody against c-Cbl (Fig. 2C). Compared to findings for untransduced and control shRNA-transduced cells, we did not observe any change in the protein levels of integrin β1 (related to KSHV entry) or Hsp70 (a well-known cellular chaperone protein) in c-Cbl shRNA-transduced cells. This suggested that our pool of c-Cbl shRNAs had minimal off-target effects (Fig. 2C). During infection, compared to untransduced and control shRNA-transduced cells, we also observed the lack of Flot-1 (LR) clustering and colocalization due to diminished protein staining in c-Cbl shRNA-transduced cells (data not shown). Moreover, control shRNA-transduced cells showed extensive colocalization between the LR marker flotillin 1 and KSHV-recognized integrin α3β1 and αVβ3 receptors (Fig. 2D, a and c), which was substantially reduced in KSHV-infected c-Cbl shRNA cells (Fig. 2D, b and d). This suggested that c-Cbl might be involved in KSHV receptor recruitment into rafts.

We have previously observed a time-dependent temporal KSHV interaction with HMVEC-d cell integrins (α3β1, αVβ3, and αVβ5) and x-CT with different patterns of association and dissociation (47); however, direct LR association of KSHV-recognized receptors was unknown. Since c-Cbl affected the LR localization of integrin receptors, we investigated the biochemical association of integrins and x-CT molecules with LRs early during infection. In uninfected endothelial cells, integrin β1 and α3 subunits were detected mainly in the NLR fractions (Fig. 3A, lane 6). In contrast, during infection, integrin β1 and α3 subunits were also detected in the LR fractions as early as 1 min p.i., which was sustained during the observed 30-min period p.i. (Fig. 3A, LR fractions). Similarly, prior to infection, integrin β3 and αV subunits were detected primarily in the NLR fractions of uninfected cells (Fig. 3B). However, infection induced a time-dependent translocation of β3 and αV into LR as early as 1 and 5 min p.i., respectively, which was gradually reduced by 10 and 30 min p.i., respectively (Fig. 3B, LR fractions). A trace amount of x-CT was associated with uninfected cell LRs (Fig. 3C). In contrast, an increased quantity of x-CT partitioned to infected cell LRs within 1 min p.i. and was detected throughout the observed 30-min p.i. period (Fig. 3C, LR fractions).

Although integrin αVβ5 has been shown to be part of a multimolecular complex of integrins and x-CT at 1 min p.i. (47), we did not observe the translocation of the β5 subunit into LRs during infection (Fig. 3D). Integrin β6 does not play a role in KSHV entry (47). Hence, the absence of β6 in LR fractions and its strict association with NLR fractions also further confirmed the specificity of α3β1, αVβ3, and x-CT detection in LR fractions (Fig. 3D). In the ligand uninduced state, epidermal growth factor receptor (EGFR) is a prototype receptor associated only with LRs (28, 34). EGFR partitioned to LRs in both the uninfected and infected HMVEC-d cells (Fig. 3E). This not only served as an appropriate receptor control for our studies but also demonstrated the specificity of infection-induced translocation of molecules that play roles in KSHV infection. The purity of LR and NLR fractions was verified by Western blot analysis for caveolin 1 and CD71, respectively (Fig. 3F).

To confirm the role of c-Cbl in receptor recruitment in rafts, we used c-Cbl shRNA-transduced cells. In untransduced and control shRNA-transduced HMVEC-d cells, integrin β1, β3, and x-CT translocated to LRs at 10 min p.i. (Fig. 3G, lanes 1 and 3), and a definite amount was also present in NLR fractions (Fig. 3G, lanes 2 and 4). However, in c-Cbl shRNA-transduced cells, we did not observe any β1, β3, or x-CT in LRs at 10 min p.i.; instead, they were strictly associated with NLRs (Fig. 3G, lanes 5 and 6). Since KSHV receptors were unable to translocate to LRs in c-Cbl shRNA-transduced cells, no KSHV (as detected by envelope glycoprotein gpK8.1A) was detected in the LRs of these cells compared to results for untransduced or control cells (Fig. 3G, lower panel, lanes 1 and 6). These results demonstrated that knocking down c-Cbl blocked the translocation of integrins β1 and β3, as well as x-CT, into LRs.

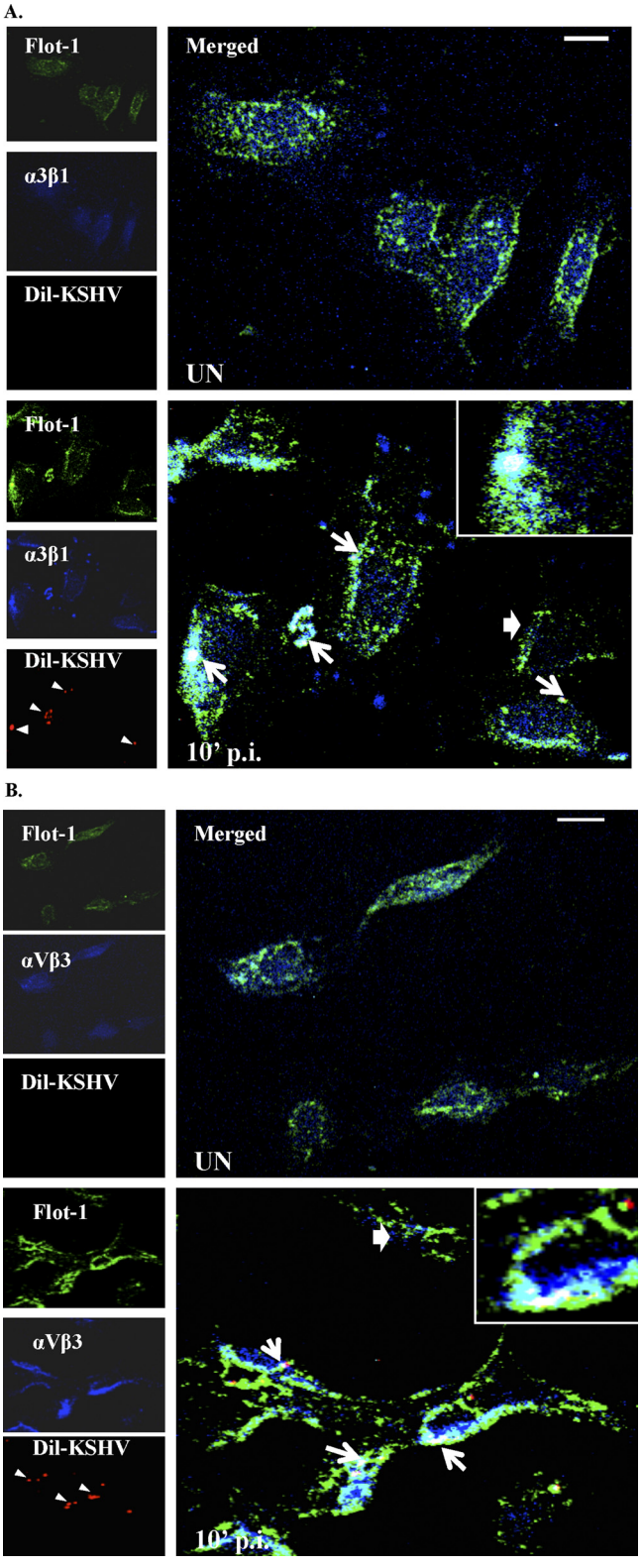

FIG. 6. Integrins and LRs colocalized in KSHV-infected cells. (A and B). Serum-starved (8 h) HMVEC-d cells were either left uninfected or infected for 10 min with Dil-KSHV, washed, and processed for immunofluorescence assay. Lipid raft and integrins (α3β1 and αVβ3) were labeled using goat anti-Flot-1 and mouse anti-integrins antibodies, respectively. They were subsequently incubated with antigoat Alexa-conjugated 488 and antimouse Alexa conjugated 405, respectively. Representative two-dimensional (2D) deconvoluted images are shown. Arrows in Dil-KSHV panels indicate infected cells. White arrows in merged panels indicate KSHV-infected cells, and colocalization and block arrows represent cells with no virus and colocalization. Scale bar, 10 μm.

Infection of HMVEC-d cells with KSHV treated with heparin, which is known to block virus binding (3), completely prevented the translocation of integrin β1 and β3, as well as x-CT, into LRs, and representative results at 10 min p.i. are shown in Fig. 3H. These results further verified the specificity of KSHV-induced receptor translocation into LRs and demonstrated that the observed receptor translocation into LRs in the infected cells is mediated by KSHV virion particles and not by any contaminating host factors.

Integrins α3β1, αVβ3, and x-CT colocalize with lipid raft markers early during KSHV infection of HMVEC-d cells. The ganglioside GM1, enriched in rafts, is widely used as a marker for LRs, and the cholera toxin B (CTxB) subunit specifically binds GM1 (30). Labeled CTxB is used to visualize GM1, and LRs appear as discrete patches on the cell periphery in fluorescence microscopy (30, 39). To further confirm the LR association of integrins and x-CT, HMVEC-d cells were either mock or KSHV infected prior to labeling with Alexa 594-conjugated CTxB. In uninfected cells, LRs appeared less clustered, and we did not observe appreciable colocalization between LR and integrin α3β1 (Fig. 4A, first panel). In contrast, α3β1 integrin colocalized with LRs at 10 min p.i. and was most notable at the edges of infected cells (Fig. 4A, second panel). When cells were infected with heparin-treated KSHV, LR clustering was reduced and colocalization between LRs and integrin α3β1 was abolished (Fig. 4A, last panel). Similar colocalizations were observed between LRs and αVβ3, as well as LRs and x-CT, at 10 min p.i., which were also abolished by heparin treatment of KSHV (Fig. 4B and C). The number of cells demonstrating colocalization between GM1 (LR) and α3β1, αVβ3, and x-CT after KSHV infection was statistically significant compared to that for uninfected cells (as indicated by the *P* values in the enlarged panels of Fig. 4A to C).

KSHV infection did not affect CTxB-recognized GM1 expression (Fig. 5A), suggesting that the intense GM1 staining observed in Fig. 4A to C is possibly due to LR coalescence during infection. Glycosylphosphatidylinositol (GPI)-anchored protein is known to be associated with LRs (18). In HMVEC-d cells transfected with GPI-GFP, integrins α3β1, αVβ3, and x-CT colocalized with GPI-GFP (LR marker) predominantly upon KSHV infection (Fig. 5B to D). In contrast, integrin αVβ5 did not colocalize with GM1 (Fig. 5E and F), further supporting its absence from LR fractions during KSHV infection (Fig. 3D).

To specifically distinguish that integrins associate with LRs (marked by Flot-1) in KSHV-infected cells, we used Dil-KSHV to track the infected cells. Compared to results for uninfected cells or cells not having viral particles, we observed the colocalization of KSHV and integrins α3β1 and αVβ3 in LRs of infected cells (Fig. 6A and B). These results clearly demonstrated that the receptor translocation events occur in KSHV-infected cells but not in cells with no KSHV.

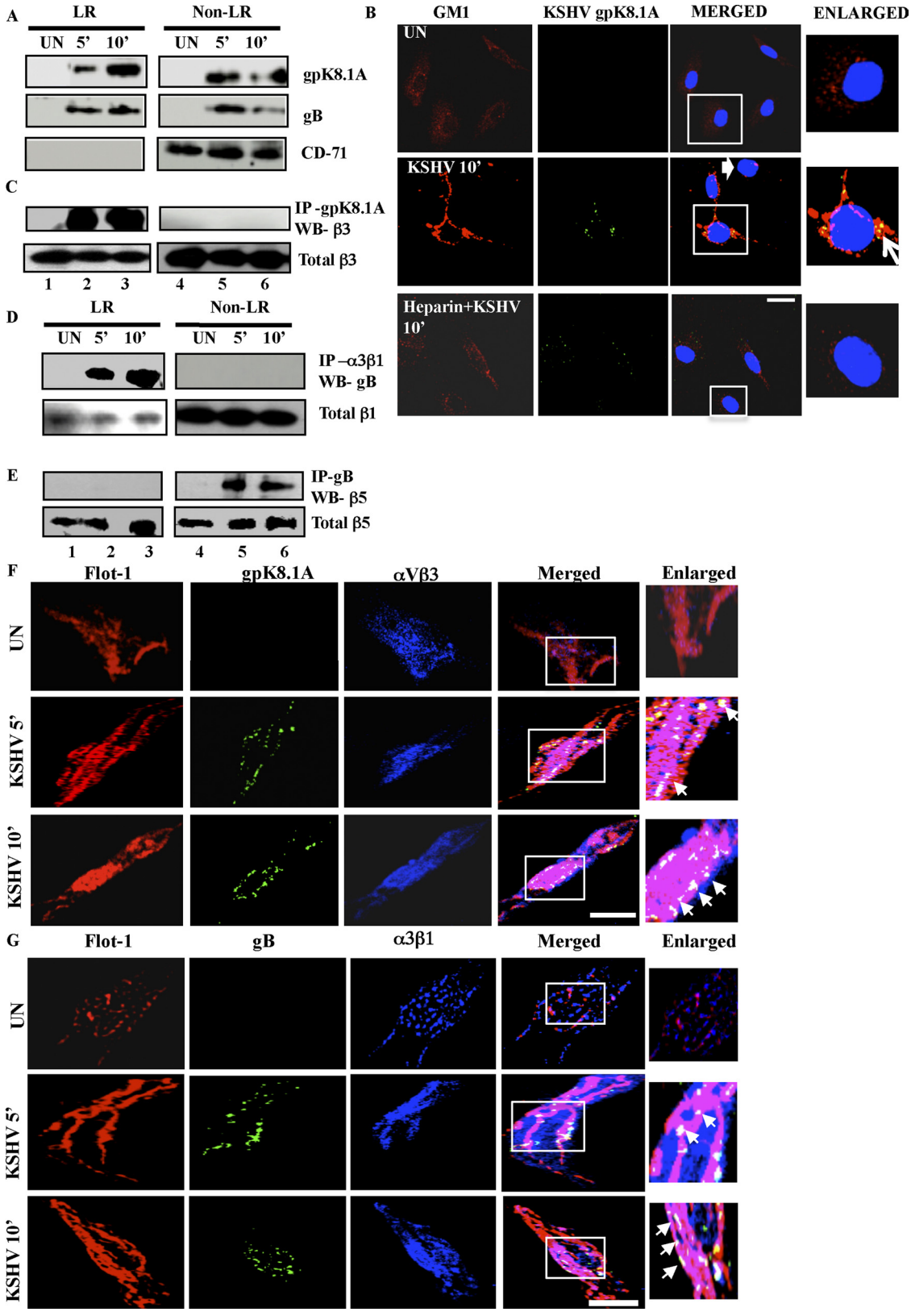

FIG. 7. Association of KSHV glycoproteins with lipid rafts early during infection of HMVEC-d cells. (A) Serum-starved (8 h) HMVEC-d cells were either left uninfected (UN) or infected with KSHV (10 DNA copies/cell) for the indicated time points and washed, and LR and non-LR fractions were prepared. Ten micrograms of protein from LR and NLR pooled fractions was subjected to Western blotting for KSHV gpK8.1A and gB. The blots were reprobed for CD-71 that is constitutively associated with non-LRs. (B) HMVEC-d cells were either left uninfected or infected for 10 min with KSHV (10 DNA copies per cell) or KSHV preincubated with heparin for 1 h at 37°C. Cells were washed three times with

KSHV envelope glycoproteins associate with lipid rafts early during KSHV infection of HMVEC-d cells. KSHV is known to bind to its target cell HS via its envelope glycoproteins gpK8.1A, gB, gH, and ORF4. Furthermore, gB is known to interact with integrins α3β1, αVβ3, and αVβ5 (2, 11, 47). To further confirm KSHV receptor-LR interactions, HMVEC-d cells were either uninfected or KSHV infected, and LR and NLR fractions were subjected to Western blotting for gpK8.1A and gB. We chose 5 and 10 min p.i. since we observed maximal LR association of α3β1, αVβ3, and x-CT during these time points. KSHV gpK8.1A was associated with LR and NLR fractions in infected endothelial cells at 5 and 10 min p.i. (Fig. 7A, LR and NLR fractions, lanes 2, 3, 5, and 6). We observed an enrichment of gpK8.1A in LR fractions at 10 min p.i. and a corresponding reduction in NLR fractions by 10 min p.i. (Fig. 7A, LR and NLR fractions). Similarly, KSHV gB showed LR association as early as 5 min p.i. and 10 min p.i. (Fig. 7A, LR fractions). KSHV gB was also associated with NLR fractions at 5 min, which was reduced by 10 min p.i. (Fig. 7A).

To further validate that localization of KSHV envelope gpK8.1A in LR occurs only during infection, we used heparin-treated virus. In contrast to results with untreated KSHV, localization of gpK8.1A with LR was abolished with heparinated KSHV (Fig. 7B). Interestingly, cells with no KSHV had less LR clustering, similar to results for uninfected cells (Fig. 7B). Moreover, heparinated KSHV-treated cells showed less LR clustering, similar to results for uninfected cells (Fig. 7B). This is consistent with our previous observations that c-Cbl shRNA and heparin treatment of KSHV prevented the translocations of KSHV and integrins into LRs (Fig. 3G and H). These results further suggested that receptor-dependent KSHV translocation into LRs is a highly virus infection-induced specific phenomenon.

Translocated integrins α3β1 and αVβ3 interact with KSHV glycoproteins in the lipid rafts. We reasoned that LRs may facilitate the viral glycoprotein-host cell receptor interaction due to its receptor clustering function. To determine the functional basis of LR-KSHV glycoprotein associations, NLR and LR fractions from uninfected and infected cells were immunoprecipitated with anti-gpK8.1A and gB antibodies and Western blotted for integrins. Integrin β3 coimmunoprecipitated (co-IPed) with gpK8.1A at 5 and 10 min p.i. only in the LR fractions (Fig. 7C, LR), and no interaction was detected in the NLR fractions (Fig. 7C, Non-LR). Similarly, the KSHV gB interaction with integrin α3β1 was detected only in the LR fractions (Fig. 7D, LR). Total β1 and β3 indicated equal loading of proteins. Very interestingly, integrin β5 was co-IPed with KSHV gB at 5 and 10 min p.i. only in the NLR fractions (Fig. 7E). Detection of α3β1 and αVβ3 exclusively in the LR fractions and the absence of αVβ5 in the LRs demonstrated that KSHV-α3β1 and -αVβ3 complexes translocated rapidly into LRs, while KSHV-αVβ5 complexes stayed in the NLR fractions.

To further confirm that KSHV utilizes LRs for interaction with α3β1 and αVβ3 integrins, we performed triple immunofluorescence staining by reacting infected HMVEC-d cells with anti-gpK8.1A, gB, flotillin 1, and integrin antibodies. In uninfected cells, we did not observe an appreciable level of colocalization between integrin αVβ3, α3β1 (blue), and LR marker flotillin 1 (red) (Fig. 7F and G, upper panel). Consistent with our observations in Fig. 7A to D, as early as 5 min p.i., KSHV (gpK8.1A) colocalized with αVβ3 in LRs (Fig. 7F, middle panel; white spots indicated by arrows) and KSHV (gB) colocalized with α3β1 in LRs (Fig. 7G, middle panel; white spots indicated by arrows). These interactions were also observed at 10 min p.i. (Fig. 7F and 7G, last panel). These results further suggested that the functional basis of enrichment of KSHV gpK8.1A and gB in LRs was indeed due to the c-Cbl-mediated translocation of KSHV-αVβ3 and KSHV-α3β1 into LRs of infected cells.

KSHV receptor integrin β1 undergoes ubiquitination facilitated by c-Cbl early during KSHV infection of HMVEC-d cells. We next sought out the molecular mechanism by which c-Cbl was aiding KSHV receptor translocation to LRs. Since c-Cbl is a very well characterized E3 ubiquitin ligase, we investigated whether it could ubiquitinate KSHV receptors during infection. It is well documented that many receptors, including tyrosine kinases, undergo ligand-dependent ubiquitination mediated by c-Cbl (44). Ubiquitination of receptors has been recognized as an internalization signal, and more importantly, the fate of receptors upon internalization varies with the pattern of ubiquitination (20, 25). We theorized that the KSHV-recruited group of related cell surface receptors may undergo c-Cbl-mediated ubiquitination early during infection.

To test our hypothesis, we first checked whether ubiquitination of the KSHV receptor α3β1 occurred during infection.

HBSS, fixed with 4% paraformaldehyde for 15 min at RT, and permeabilized with 0.2% Triton X-100 for 5 min at RT. Cells were blocked with signal enhancer for 20 min and stained for GM1 by incubating with Alexa 594-conjugated CTxB for 45 min at 4°C, washed three times with chilled HBSS, and incubated with anti-CTB for 45 min at 4°C. These lipid raft labeled cells were costained with mouse anti-gpK8.1A monoclonal antibody for 1 h at RT followed by Alexa 488 anti-mouse antibody for 1 h at RT. The boxed area is represented in the enlarged panel, and the block arrow denotes a cell lacking KSHV. The arrow in the enlarged panel indicates colocalization. Scale bar, 10 μm. (C, D, and E) Two hundred micrograms of protein from LR and NLR fractions were immunoprecipitated with either anti-gpK8.1A antibody, anti-integrin α3β1 antibody, or anti-KSHV gB antibody for 2 h at 4°C and subjected to Western blotting for integrin β3 (C), KSHV gB (D), or integrin β5 (E). Ten micrograms of protein from whole-cell lysates was used for Western blotting for integrin β3 (C), integrin β1 (D), or β5 (E) as a loading control. (F and G) Serum-starved (8 h) HMVEC-d cells were either mock infected or KSHV infected (10 DNA copies/cell) for the indicated time points. Cells were labeled for LR using Flot-1 primary antibody followed by Alexa 594 (red) secondary antibody. (F) Lipid raft labeled cells were costained with rabbit anti-integrin αVβ3 monoclonal antibody followed by Alexa 405 (blue) antirabbit secondary antibody; subsequently, cells were stained with mouse anti-gpK8.1A monoclonal antibody for 1 h at RT followed by Alexa 488 (green) antimouse antibody. (G) Lipid raft labeled cells were costained with rabbit polyclonal anti-gB antibody for 1 h at RT followed by Alexa 488 anti-rabbit antibody for 1 h at RT; subsequently, cells were stained with mouse anti-integrin α3β1 antibody for 1 h at RT followed by Alexa 405 secondary antibody for 1 h at RT. Representative 2D deconvoluted images processed by Metamorph software are shown. Boxed areas are enlarged in the rightmost panels. Arrows in enlarged panels indicate colocalization. Scale bar, 10 μm.

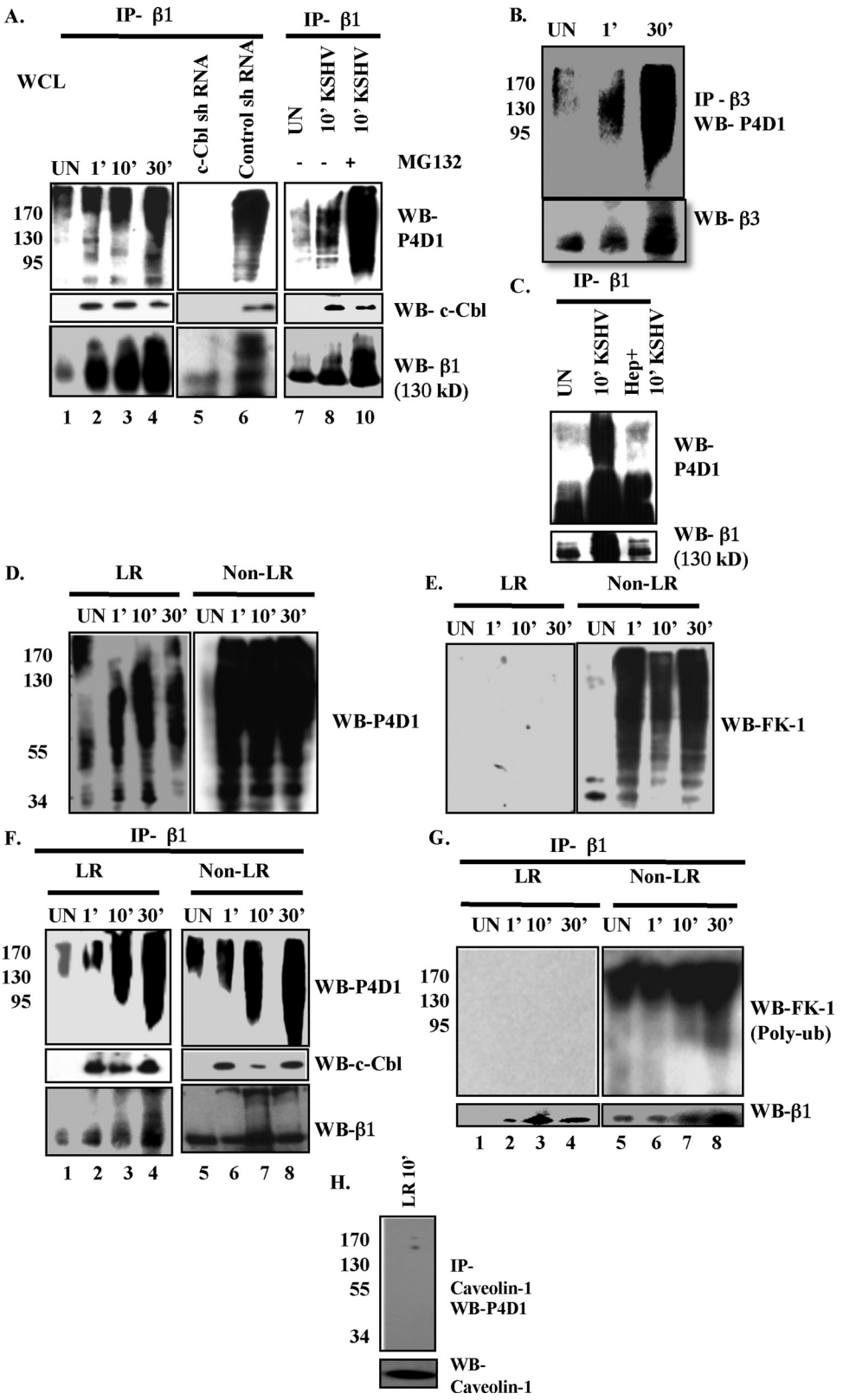

FIG. 8. Differential c-Cbl-mediated ubiquitination of integrins early during KSHV infection of HMVEC-d cells. (A) Untransduced, control shRNA- and c-Cbl shRNA lentivirus-transduced HMVEC-d cells were either pretreated with 10 μM MG132 for 6 h at 37°C or left untreated. After washing, cells were mock or KSHV infected (10 DNA copies/cell) for the indicated time points. Cells were lysed using sodium bicarbonate buffer (pH 11), and 200 μg protein of untransduced whole-cell lysates (WCL) was immunoprecipitated with mouse anti-β1 monoclonal antibody for 2 h at 4°C and subjected to Western blotting for total ubiquitin by P4D1 (mouse antimono- and antipolyubiquitin monoclonal antibody). The same

We immunoprecipitated uninfected or KSHV-infected HMVEC-d whole-cell lysates (WCL) with β1 antibody and Western blotted using P4D1 monoclonal antibody against ubiquitin, which is known to efficiently recognize both mono- and polyubiquitin (15). We also used FK-1 monoclonal antibodies, which specifically detect polyubiquitin but not monoubiquitin (15). Compared to uninfected cells, increased mono- and polyubiquitination of β1 (smeary band pattern) was detected by P4D1 antibody as early as 1 min p.i. and throughout the observed 30 min p.i. (Fig. 8A, upper left panel, lanes 1 to 4). To determine whether during infection c-Cbl is involved in interaction with α3β1 and its ubiquitination, β1 immunoprecipitate was Western blotted for c-Cbl. The interaction of c-Cbl with β1 was detected from 1 min p.i. until 30 min p.i. (Fig. 8A, middle left panel, lanes 1 to 4). When the blot was stripped and reprobed for integrin β1, compared to results for uninfected cells, we observed smeary band patterns in the infected cells (Fig. 8A, bottom left panel, lanes 1 to 4). Similar results were also seen with β3 integrin (Fig. 8B).

Mono- and polyubiquitination of β1 was also observed in control shRNA-transduced KSHV-infected cells (Fig. 8A, upper middle panel, lane 6). In contrast, no β1 ubiquitination was observed in c-Cbl shRNA-transduced cells (Fig. 8A, lane 5). We also detected a similar smeary mono- and poly-β1 ubiquitination pattern in control shRNA cells but not in c-Cbl shRNA-transduced cells (Fig. 8A, bottom middle panel, lanes 5 and 6). Moreover, inhibition of proteasomal degradation by MG132 also increased mono- and polyubiquitination, as well as accumulation of ubiquitinated β1 (Fig. 8A, lanes 7 to 10). These exciting results suggested that c-Cbl promotes the ubiquitination of α3β1 early during infection.

To prove that integrin β1 ubiquitination is a result of KSHV infection, we used heparin-treated KSHV for infection. As expected, integrin β1 ubiquitination was significantly reduced by heparin treatment of KSHV, suggesting that KSHV binding in infected cells triggers the ubiquitination of KSHV receptors (Fig. 8C).

We observed the presence of both mono- and polyubiquitin molecules (as detected by P4D1 and FK-1) in the total LR and NLR fractions from uninfected and infected cells, with intense smeary patterns resembling polyubiquitin in NLR fractions (Fig. 8D and E). Intense smeary FK-1 reactivity in NLR fractions after infection further supported the presence of more polyubiquitination targets in NLR than in LRs (Fig. 8D and E). Next, we used immunoprecipitation to determine whether β1 ubiquitination occurred in the LR and/or NLR part of the membranes. In infected cells, we observed ubiquitination of β1 in both LR and NLR fractions (Fig. 8F, upper panel, lanes 1 to 8). We observed moderate ubiquitination of β1 in uninfected LR fractions, but KSHV infection promoted more ubiquitination at 10 min and 30 min p.i. (Fig. 8F, upper left panel, lanes 1 to 4). The varied levels of expression and ubiquitination of β1 are possibly proportionate to the degree of receptor translocation into the LR. When the LR and NLR fractions were immunoprecipitated with anti-β1 antibodies and Western blotted for c-Cbl, we did not detect c-Cbl in the uninfected cells. In contrast, a prominent level of c-Cbl was detected as early as 1 min p.i., until 30 min p.i., in both LR and NLR fractions of infected cells (Fig. 8F, middle panel). These observations indicated that c-Cbl interacted with integrin β1 in both LR and NLR fractions and possibly mediated ubiquitination during primary KSHV infection. The integrin β1 blot showed a smeary pattern resembling ubiquitination in KSHV-infected cells in LR and NLR fractions compared to results for uninfected cells (Fig. 8F, lower panel).

Differential ubiquitination of KSHV receptor is observed in lipid rafts and nonrafts early during KSHV infection of HMVEC-d cells. Since these results demonstrated that integrin β1 ubiquitination mediated by c-Cbl occurred in both LR and NLR fractions, we next examined whether there were any differences in the integrin ubiquitination pattern between LR and NLR regions of the plasma membranes. Evidences showing that receptor monoubiquitination is involved in endocytosis and internalization while polyubiquitination leads to receptor degradation are well documented (15, 46). Hence, we characterized the differential ubiquitination pattern of β1 in the LR and NLR fractions. Upon immunoprecipitating integrin β1 from both KSHV-infected LR and NLR fractions, we observed that FK-1 did not show any reactivity with integrin β1 in LR fractions (Fig. 8G, upper left panel), and in striking contrast, FK-1 reacted with β1 in NLR fractions (Fig. 8G, upper right panel). This suggested that the observed smeary ubiquitination pattern of integrin β1 in LR could be due to monoubiquitination at several sites (15) but it was polyubiquitinated in NLR fractions (Fig. 8G). We verified that this receptor ubiquitination was specific for KSHV-induced translocated integrin β1, since caveolin 1, an abundant protein marker of lipid rafts, did not undergo similar ubiquitination post-KSHV infection (Fig. 8H).

lysates were immunoprecipitated with mouse anti-β1 monoclonal antibody for 2 h at 4°C and subjected to Western blotting for total c-Cbl. The blot was stripped and reprobed for integrin β1. (B) Uninfected or KSHV-infected WCL were immunoprecipitated with anti-β3 antibody for 2 h at 4°C. After washing 3 times with 1× PBS, samples were prepared for Western blotting with P4D1 antibody. The blot was stripped and reprobed for β3. (C) Serum-starved HMVEC-d cells were either mock or KSHV infected. For heparin treatment of KSHV, KSHV was preincubated with 50 mg/ml of heparin for 1 h at 37°C and used for infecting cells for 10 min. Cell lysates were immunoprecipitated with anti-β1 antibody and Western blotted for total ubiquitin using P4D1 antibody. (D and E) LR and NLR fractions isolated from either mock- or KSHV-infected serum-starved HMVEC-d cells were subjected to Western blotting with P4D1 antibody detecting total (mono- and poly-) ubiquitination (D) or with FK-1 antibody detecting polyubiquitination (E). (F and G) Serum starved (8 h) HMVEC-d cells were either mock or KSHV infected (10 DNA copies/cell) for the indicated time points. Two hundred micrograms of LR and NLR proteins were immunoprecipitated with anti-β1 antibodies for 2 h at 4°C followed by Western blotting using P4D1 (F) or FK-1 (G) antibodies. The blots were stripped and reprobed for integrin β1. The same lysates were immunoprecipitated with anti-β1 antibody for 2 h at 4°C and subjected to Western blotting for total c-Cbl (F). (H) Two hundred micrograms of protein LR fractions of KSHV-infected HMVEC-d cells were immunoprecipitated with anticaveolin antibody, followed by Western blotting for P4D1. The blot was stripped and reprobed for caveolin 1.

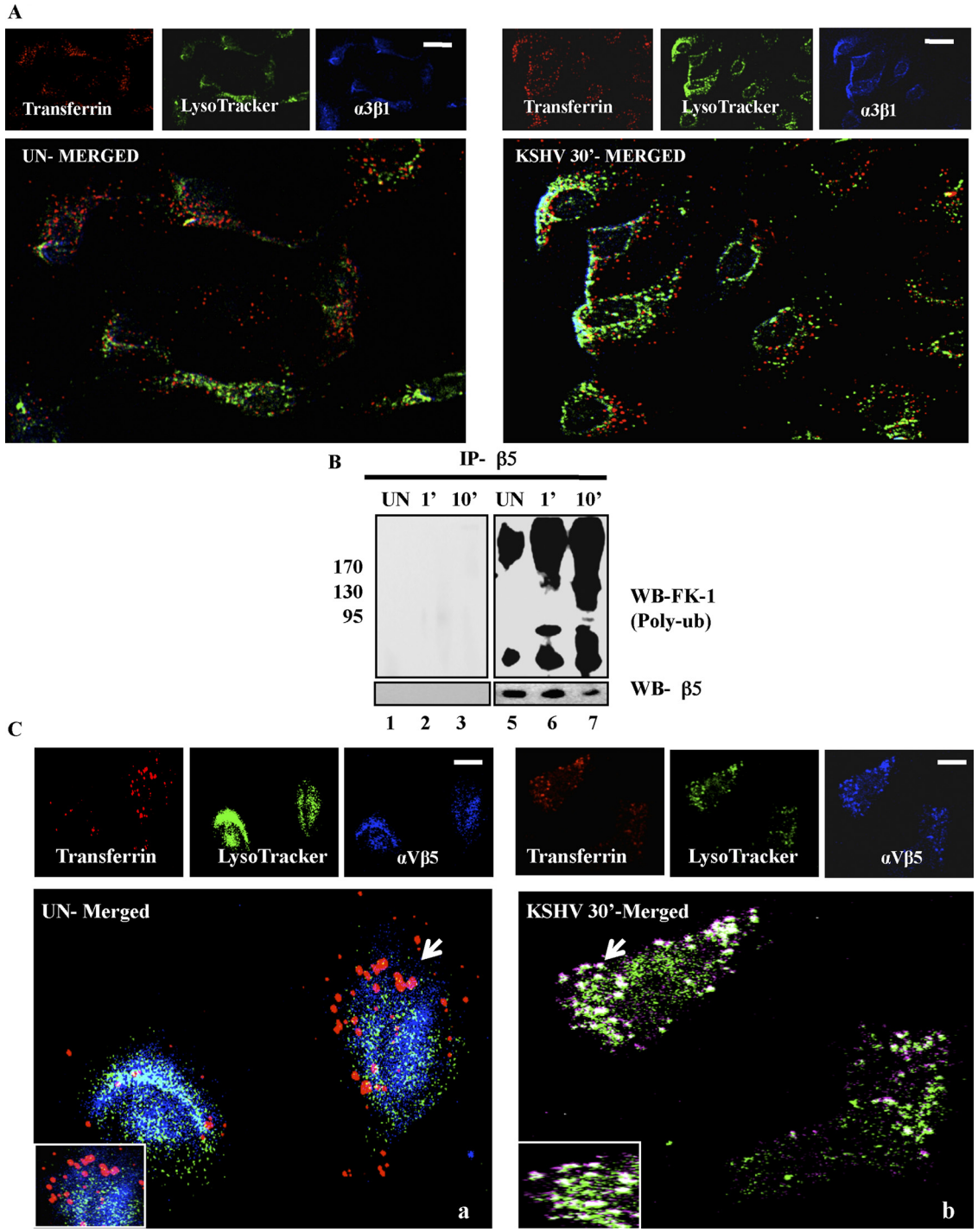

FIG. 9. Integrin αVβ5 but not α3β1 associates with the clathrin marker transferrin during KSHV infection of HMVEC-d cells. (A) HMVEC-d cells were incubated with medium containing Texas Red-labeled transferrin and LysoTracker green along with KSHV at 37°C for 30 min. Cells were processed for immunofluorescence analysis using anti-integrin α3β1 antibody followed by Alexa 405 anti-mouse secondary antibody. Scale bar, 10 μm. (B) Serum-starved (8 h) HMVEC-d cells were either mock or KSHV infected (10 DNA copies/cell) for the indicated time points. Two hundred micrograms of LR and NLR proteins were immunoprecipitated with anti-β5 antibodies for 2 h at 4°C, followed by Western blotting using FK-1 antibody. The blot was stripped and reprobed for integrin-β5. (C) HMVEC-d cells were incubated with serum-free medium containing Texas Red-labeled transferrin or dextran and LysoTracker green along with KSHV at 37°C for 30 min. Cells were processed for immunofluorescence analysis using anti-integrin αVβ5 antibody followed by Alexa 405 anti-mouse secondary antibody. Bottom panels represent merged and enlarged views. Arrows indicate colocalization and the area enlarged. Scale bar, 10 μm.

LR-translocated integrin α3β1 is not targeted to lysosomes, while non-LR-partitioned integrin αVβ5 is targeted toward clathrin-dependent targeting to lysosomes. HMVEC-d cells were incubated with transferrin, a physiological ligand known to enter cells via clathrin-dependent endocytosis, and LysoTracker. In uninfected and infected cells, no appreciable colocalization between integrin α3β1, transferrin, and LysoTracker was observed (Fig. 9A). This suggested that KSHV bound to α3β1 was not trafficked toward lysosomes via clathrin-mediated endocytosis, thereby facilitating a productive infection.

Since KSHV also interacted with αVβ5, which stayed in the NLR fractions of infected cells, we next examined the fate of virus bound to αVβ5. Non-LR partitioned integrin β5 was increasingly polyubiquitinated (as detected by FK-1 antibody) during KSHV infection compared to uninfected cells (Fig. 9B, lanes 5 to 7). No significant colocalization of αVβ5 with transferrin and LysoTracker was observed in uninfected cells (Fig. 9C, panel a). In contrast, we observed the colocalization of αVβ5 with transferrin and LysoTracker in KSHV-infected cells (Fig. 9C, panel b). This supports our earlier observation that polyubiquitinated non-LR-partitioned αVβ5 is targeted toward lysosomes.

c-Cbl knockdown and LR disruption alter the endocytic route and target KSHV toward lysosomes. As in our previous study (45), c-Cbl shRNA reduced the entry of KSHV and viral gene expression in HMVEC-d cells (data not shown). Though about 20% of initial input virus entered the target cells, a >90% reduction in viral gene expression was observed (45). Here we sought to determine the mechanism by which c-Cbl affected the fate of KSHV endocytosis and trafficking and the fate of KSHV that entered during c-Cbl knockdown. We tracked the entry of KSHV along with transferrin, or dextran in control and c-Cbl shRNA-transduced cells. In control cells, KSHV did not colocalize appreciably with transferrin and was not observed in lysosomes (Fig. 10A, panels b and d and insets). However, c-Cbl shRNA-transduced cells showed significant colocalization between KSHV and transferrin (Fig. 10A, panels f and h and insets). Additionally, in c-Cbl shRNA cells, KSHV endocytosed by the clathrin pathway accumulated in lysosomal degradation compartments with 84% colocalization frequency (Fig. 10A, panel h, inset, white spots, and B). These results suggested that even though some level of KSHV entered the target cells, it did not result in a productive infection since when c-Cbl was knocked down, KSHV was internalized by the clathrin dependent pathway and was targeted to lysosomes.

We next rationalized that if c-Cbl-mediated translocation of receptor-associated KSHV into LRs was crucial for macropinocytosis-based productive infection, then disruption of LRs by cholesterol sequestrating MβCD should inhibit infection. Therefore, we determined the fate of KSHV in LR-disrupted cells by tracking virus with LysoTracker. During KSHV infection of untreated HMVEC-d cells, we did not observe appreciable colocalization between virus and LysoTracker (Fig. 10C), indicating that KSHV was minimally associated with lysosomal compartments. However, upon MβCD treatment we observed that most of the virus particles that entered the cells were associated with lysosomal compartments (Fig. 10D). Triple immunofluorescence studies involving KSHV, transferrin or dextran, and LysoTracker confirmed that KSHV did not colocalize appreciably with transferrin and lysosomes (Fig. 10E, panels a to e, and B). In contrast, extensive colocalization between virus and dextran was observed in untreated cells (Fig. 10E, panels k to m). However, upon LR disruption, we observed significant colocalization between KSHV and transferrin (Fig. 10E, panel h, inset), and in contrast, KSHV did not colocalize with the macropinocytosis marker dextran (Fig. 10E, panel r). Additionally, KSHV endocytosed by the clathrin pathway accumulated in lysosomal compartments with 78% colocalization frequency (Fig. 10E, panel j, inset white spots, and B). Furthermore, MβCD treatment also prevented the c-Cbl-mediated translocations of KSHV-associated integrin β1, β3, and x-CT molecules (Fig. 10F), suggesting the importance of raft integrity in addition to c-Cbl during KSHV receptor interactions.

We next analyzed the expression of punctate nuclear LANA-1 after 48 h p.i. during c-Cbl knockdown and LR disruption. In conjunction with our earlier studies (36, 45), we observed 91% and 80% reduction in LANA-1 expression by c-Cbl shRNA and MβCD treatment, respectively (Fig. 11A). Taken together, our studies demonstrated that c-Cbl and LR are essential components in KSHV infection via macropinocytosis, which results in a productive infection leading to establishment of latency in infected cells.

DISCUSSION

LR roles vary according to virus and cell type since they are dictated by several factors, such as the association of contact and entry receptor(s) with LRs, the mode of viral entry, the role of the LR in fusion of the enveloped virus membrane with cellular membranes, LR-associated signal molecules and their activation, the consequences of such activation, and downstream molecules. Though cell surface receptor translocation into LRs has been shown for many enveloped and nonenveloped viruses (5, 31, 32, 51), the mechanism behind this translocation is not known. Our present studies with the KSHV model suggest that c-Cbl plays an active role in the translocation of a subset of KSHV-recognized receptors into LR (Fig. 11B). Our comprehensive biochemical and morphological studies elucidated the role of c-Cbl in recruitment of KSHV-recognized cell surface receptors into lipid rafts. We provide the evidence that c-Cbl-mediated selective virus-receptor translocations and differential ubiquitination in rafts are critical determinants of the macropinocytic entry route and productive infection of KSHV.

Our biochemical results show that most of the currently identified cell surface molecules recognized by KSHV, such as HS, α3β1, αVβ3, αVβ5, and x-CT, are not strictly LR-resident molecules. Infection-activated c-Cbl induces the rapid selective translocation of α3β1, αVβ3, and x-CT molecules into the LR. The ability of c-Cbl shRNA treatment to block the LR translocation of virus, β1, β3, and x-CT molecules clearly suggests that c-Cbl mediates the LR translocation of these selected molecules, potentially for monoubiquitination in the LR. The occurrence of distinct LR clustering with GM1 and Flot-1 immunostaining during KSHV infection is a clear indication of raft-dependent signaling and receptor activation that has been

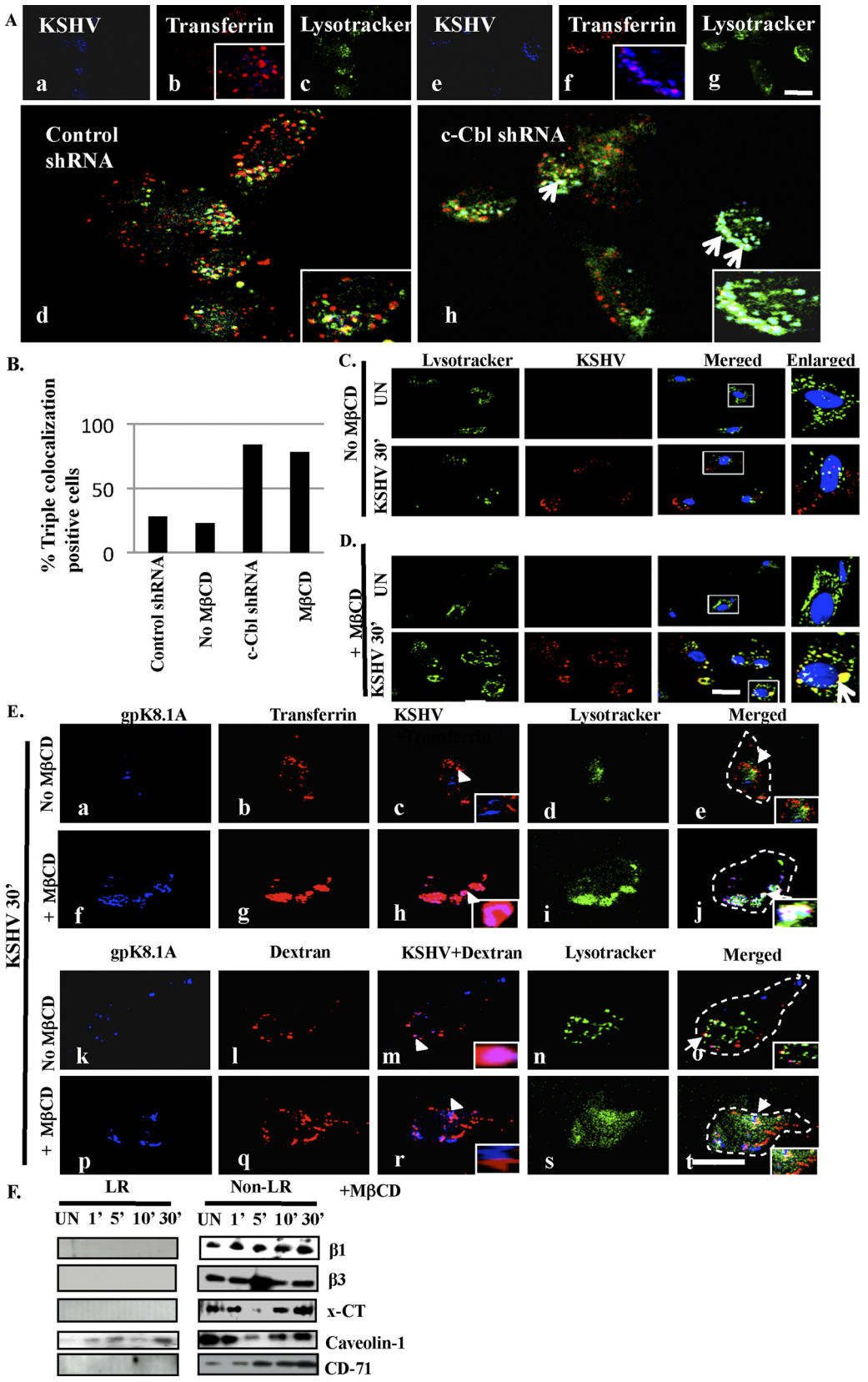

FIG. 10. Effect of c-Cbl knockdown and LR disruption on the endocytic route of KSHV. (A) Control and c-Cbl shRNA-transduced cells were incubated with medium containing Texas Red-labeled transferrin or dextran and LysoTracker green along with KSHV at 37°C for 30 min. Cells were processed for immunofluorescence analysis using anti-gpK8.1A antibody followed by Alexa 405 antimouse secondary antibody. Arrows in panel h indicate the area of the cell enlarged and represented in the inset. (B) The percentage of cells bearing triple colocalization was calculated

described previously (52). A recent study also demonstrated a similar clustering of GM1-rich LRs by influenza virus (9).

Cbl proteins are known to play important roles in signal transduction as negative regulators of receptor-based signaling by promoting ubiquitination (40). The Cbl proteins are responsible for ubiquitinating activated tyrosine kinases and targeting them for degradation. In addition to our recent report of c-Cbl regulation in macropinocytosis-dependent entry of KSHV (45), we now show that c-Cbl functions as an E3 ubiquitin ligase during early infection and ubiquitinates KSHV integrin receptor α3β1. c-Cbl utilizes LRs for differential ubiquitination during infection. Although c-Cbl ubiquitinylated β1 in both LR and non-LR fractions, there were considerable differences in the ubiquitination patterns. Integrin β1 is monoubiquitinated in the LR, potentially for endocytosis and internalization, whereas the same integrin in the non-LR is polyubiquitinated, suggesting the possibility of targeting toward degradation. Polyubiquitination of certain receptors has been shown to be followed by receptor internalization and degradation in lysosomes (46). Similarly, multiple monoubiquitinated and polyubiquitinated proteins can be endocytosed efficiently and targeted toward lysosomal/proteasomal degradation (14).

The fact that αVβ5 was not recruited to LRs by c-Cbl is very interesting. Our studies have shown that polyubiquitinated αVβ5- but not α3β1-associated KSHV is targeted toward lysosomes during HMVEC-d cell infection. The partition of αVβ5-bound KSHV virions into the lysosomal compartments in LR intact cells, as well as the accumulation of KSHV in lysosomes that entered during c-Cbl knockdown and LR disruption (MβCD) and the drastic reduction in LANA-1 expression, are suggestive of segregation of productive and nonproductive pathways during infection. Though destruction of KSHV particles in the lysosomes is presumed here, further studies are required to demonstrate the destruction of KSHV in lysosomal compartments. These studies include the isolation of lysosomes at different times p.i. from c-Cbl knockdown cells, as well as intact and disrupted LR cells, and assaying for the presence of infectious KSHV. Such studies are beyond the scope of the present study and need to be pursued further.

Similarly, the segregation of signaling induced between LR-translocated integrin-KSHV and non-LR-partitioned αVβ5-KSHV is a promising future study. Whether KSHV interacting with integrin αVβ5 initiates the induction of the FAK/Src pathway and the nature of signal pathways that are exclusively induced by the KSHV-LR-α3β1, -αVβ3, and -x-CT- complexes need further evaluation. Additionally, the possibilities of a novel endosomal molecular partner(s) in mediating ubiquitination, followed by internalization upon viral infection, cannot be ruled out.

Early during infection of HMVEC-d cells, KSHV was also associated with non-LR fractions since they were also enriched with entry receptors. This indicates that LRs and associated molecules, such as c-Cbl, may selectively delineate KSHV-bound receptors, possibly for different endocytic fates of the virus. Similar non-LR-associated HIV-1 receptors are also reported during infection (35). Our studies raise an important question: why does a subpopulation of KSHV receptors translocate to the LR? The most probable answer is that the receptor translocation event may generate advantages for KSHV in establishing infection. Owing to the receptor clustering ability of LRs, KSHV glycoproteins are probably in near-physical contact with aggregated translocated receptors. Second, c-Cbl-mediated monoubiquitination may be facilitating the efficient internalization and endocytosis of KSHV in LRs, while polyubiquitination of receptor-associated virus in non-LRs may be targeted toward lysosomes. c-Cbl-mediated receptor translocation probably facilitates LRs to act as a signaling matrix. This is supported by our data, where loss of c-Cbl function abolished the association of KSHV and its receptors with LRs. Our previous studies indicated that LR disruption increased Src activation and viral entry (36). This is supported by our current study, where increased viral entry is attributed to lysosomal targeting. Moreover, c-Cbl knockdown and LR disruption led to switching of the endocytic route followed by lysosomal targeting, strongly suggesting that both c-Cbl and cholesterol-rich lipid rafts were crucial for KSHV productive endocytosis.

The requirement for translocation of KSHV-bound receptors into the LR for productive macropinocytic entry of KSHV and localization of LR-associated c-Cbl at the junction of bleb formation emphasizes a complex role for c-Cbl and LRs. c-Cbl and its associated proteins are known to be part of a complex signaling interactome controlling a variety of functions, including internalization and endosomal sorting (24, 40). c-Cbl may potentially associate with other endosomal sorter proteins enforcing the internalization of LR-bound host cell receptors associated with KSHV postmonoubiquitination while allowing the lysosomal targeting of non-LR-bound KSHV mediated by polyubiquitination. Whether c-Cbl and its interacting molecular partners remain associated with internalized KSHV-bound receptors regulating the endosomal sorting process requires further analysis.

Overall, our study reveals that c-Cbl-mediated translocations of KSHV and selected receptors (α3β1, αVβ3, and x-CT

in three independent fields having at least 10 cells per field. (C and D) HMVEC-d cells grown in chamber slides were either pretreated with 5 mM MβCD for 1 h at 37°C or left untreated. Cells were incubated with medium containing LysoTracker with or without KSHV for 30 min at 37°C and processed for immunofluorescence assay using mouse anti-KSHV gpK8.1A monoclonal antibody for 1 h at RT followed by incubation with Alexa 594 anti-mouse antibody for 1 h at RT. 2D deconvoluted images were acquired using a fluorescence microscope. The boxed areas indicate the area of the cell enlarged, and arrows in the enlarged panel indicate colocalization; the scale bar represents 10 μm. (E) HMVEC-d cells treated same as in panels C and D and incubated with medium containing Texas Red-labeled transferrin or dextran and LysoTracker green along with KSHV at 37°C for 30 min. Cells were processed for immunofluorescence analysis using anti-gpK8.1A antibody followed by Alexa 405 anti-mouse secondary antibody. The scale bar represents 10 μm. Arrowheads in panels c, h, l, and q represent the area of cell enlarged and shown in the inset. Arrows in the merged panels of E represent the area of the cell enlarged, shown in the inset. The dotted line in the merged panel represents the cell boundary. Scale bar, 10 μm. (F) Serum-starved HMVEC-d cells were pretreated with MβCD for 1 h at 37°C. After washing out the drug, LR and non-LR fractions were isolated as described previously and subjected to Western blotting for the indicated proteins.

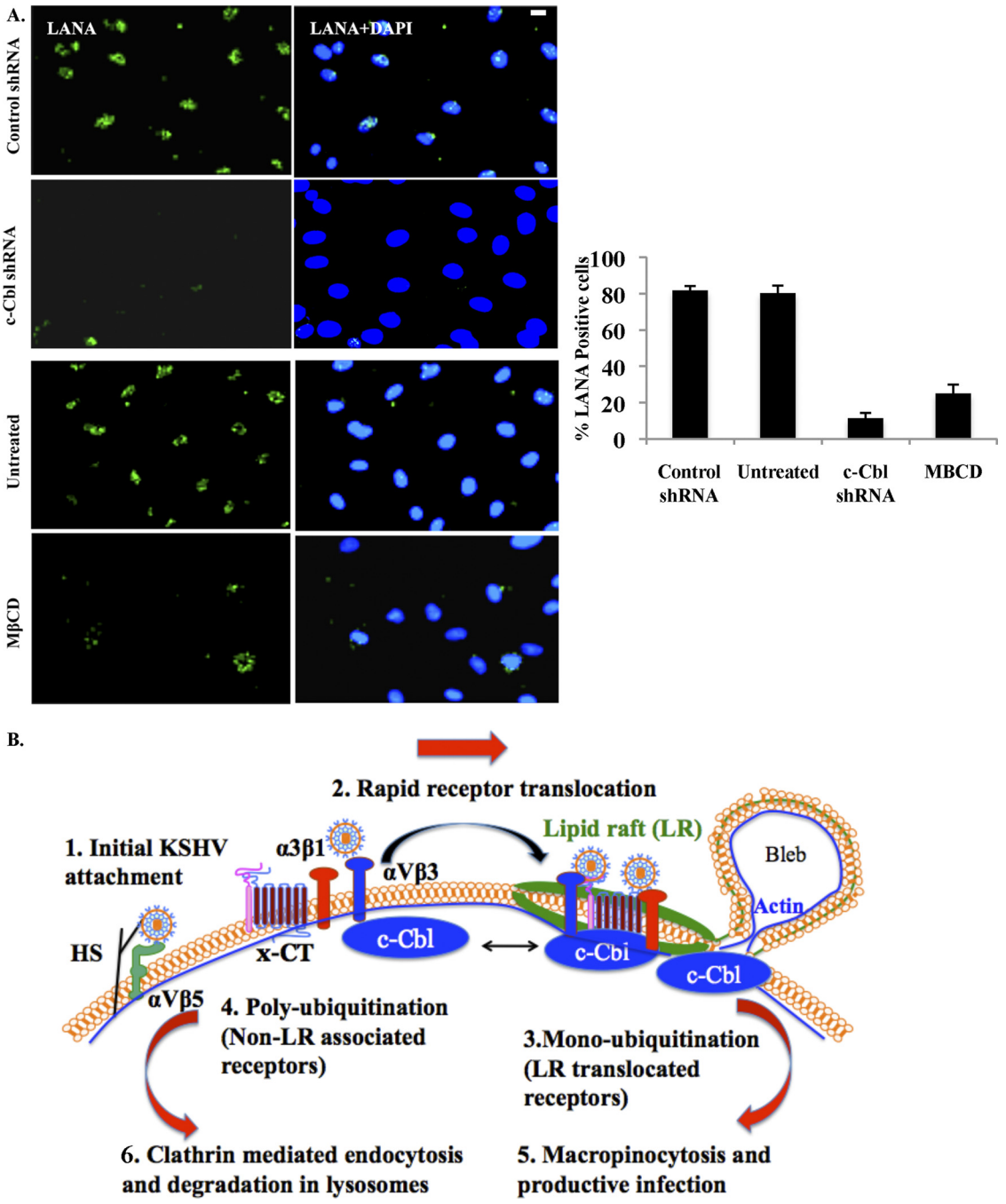

FIG. 11. c-Cbl and LR regulate the establishment of productive KSHV infection. (A) Control or c-Cbl shRNA-transduced HMVEC-d cells were mock or KSHV infected (10 DNA copies/cell) for 2 h. For LR disruption, cells were pretreated with 5 mM MβCD as before. After washing and virus removal, cells were cultured in complete medium for another 46 h. After washing, cells were fixed and processed for immunofluorescence assay using anti-LANA-1 antibody. Representative images are shown. Scale bar, 10 μm. The percentage of cells showing punctate LANA-1 dots is represented in the graphical plot. A minimum of 3 fields having at least 20 cells were chosen. Error bars show ± SD. (B) Model showing the dynamic sequence of early events of KSHV infection of HMVEC-d cells and potential mechanism of KSHV-induced receptor translocation into the lipid raft for promotion of different endocytic and postendocytic virus fates. Initial KSHV interactions with heparan sulfate (HS) and α3β1, αVβ3, and αVβ5 integrins occurs in the NLR regions of the membranes (1), which is followed by (2) c-Cbl-mediated selective rapid translocation of KSHV into the LR along with the α3β1, αVβ3, and x-CT receptors but not αVβ5. KSHV-associated αVβ5 remains in the NLR parts of the membranes. Activated c-Cbl localizes with LRs at the junctional base of macropinocytic blebs (3). c-Cbl-mediated monoubiquitination of translocated receptors is followed by productive macropinocytic entry (3 and 4). Non-LR-partitioned KSHV-bound receptor is polyubiquitinated and directed to a clathrin-dependent lysosomal nonproductive pathway along with KSHV (5 and 6). c-Cbl knockdown blocks the macropinocytosis and receptor translocation, and diverts KSHV to a clathrin-lysosomal noninfectious pathway (5 and 6). LR disruption also blocks receptor translocation and diverts KSHV to a clathrin-lysosomal noninfectious pathway (5 and 6).

molecules) into LRs via monoubiquitination followed by macropinocytosis results in a productive infection (Fig. 11B). This suggests that targeting c-Cbl and LRs can potentially control KSHV infection of dermal endothelial cells.

ACKNOWLEDGMENTS

This study was supported in part by Public Health Service grant CA 075911 and a Rosalind Franklin University of Medicine and Science H. M. Bligh Cancer Research Fund grant to B.C.

We thank Alice Gilman-Sachs and Keith Philibert for critically reading the manuscript. We thank Kai Simons, Max-Planck-Institute of Molecular Cell Biology and Genetics, Dresden, Germany, for the generous gift of the GPI-GFP plasmid.

REFERENCES

1. **Akula, S. M., N. P. Pramod, F. Z. Wang, and B. Chandran.** 2001. Human herpesvirus 8 envelope-associated glycoprotein B interacts with heparan sulfate-like moieties. Virology **284:**235–249.
2. **Akula, S. M., N. P. Pramod, F. Z. Wang, and B. Chandran.** 2002. Integrin alpha3beta1 (CD 49c/29) is a cellular receptor for Kaposi's sarcoma-associated herpesvirus (KSHV/HHV-8) entry into the target cells. Cell **108:**407–419.
3. **Akula, S. M., F. Z. Wang, J. Vieira, and B. Chandran.** 2001. Human herpesvirus 8 interaction with target cells involves heparan sulfate. Virology **282:**245–255.
4. **Birkmann, A., et al.** 2001. Cell surface heparan sulfate is a receptor for human herpesvirus 8 and interacts with envelope glycoprotein K8.1. J. Virol. **75:**11583–11593.
5. **Carter, G. C., et al.** 2009. HIV entry in macrophages is dependent on intact lipid rafts. Virology **386:**192–202.
6. **Cesarman, E., Y. Chang, P. S. Moore, J. W. Said, and D. M. Knowles.** 1995. Kaposi's sarcoma-associated herpesvirus-like DNA sequences in AIDS-related body-cavity-based lymphomas. N. Engl. J. Med. **332:**1186–1191.
7. **Chandran, B.** 2010. Early events in Kaposi's sarcoma-associated herpesvirus infection of target cells. J. Virol. **84:**2188–2199.
8. **Chang, Y., et al.** 1994. Identification of herpesvirus-like DNA sequences in AIDS-associated Kaposi's sarcoma. Science **266:**1865–1869.
9. **Eierhoff, T., E. R. Hrincius, U. Rescher, S. Ludwig, and C. Ehrhardt.** 2010. The epidermal growth factor receptor (EGFR) promotes uptake of influenza A viruses (IAV) into host cells. PLoS Pathog. **6**(9):e1001099.
10. **Ganem, D.** 2007. Kaposi's sarcoma-associated herpesvirus, p. 2875–2888. *In* D. M. Knipe et al. (ed.), Fields virology, 5th ed., vol. 2. Lippincott Williams & Wilkins, Philadelphia, PA.
11. **Garrigues, H. J., Y. E. Rubinchikova, C. M. Dipersio, and T. M. Rose.** 2008. Integrin alphaVbeta3 binds to the RGD motif of glycoprotein B of Kaposi's sarcoma-associated herpesvirus and functions as an RGD-dependent entry receptor. J. Virol. **82:**1570–1580.
12. **Giancotti, F. G., and G. Tarone.** 2003. Positional control of cell fate through joint integrin/receptor protein kinase signaling. Annu. Rev. Cell Dev. Biol. **19:**173–206.
13. **Gorvel, J. P., P. Chavrier, M. Zerial, and J. Gruenberg.** 1991. rab5 controls early endosome fusion in vitro. Cell **64:**915–925.
14. **Haglund, K., P. P. Di Fiore, and I. Dikic.** 2003. Distinct monoubiquitin signals in receptor endocytosis. Trends Biochem. Sci. **28:**598–603.
15. **Haglund, K., et al.** 2003. Multiple monoubiquitination of RTKs is sufficient for their endocytosis and degradation. Nat. Cell Biol. **5:**461–466.
16. **Hahn, A., et al.** 2009. Kaposi's sarcoma-associated herpesvirus gH/gL: glycoprotein export and interaction with cellular receptors. J. Virol. **83:**396–407.
17. **Harder, T., P. Scheiffele, P. Verkade, and K. Simons.** 1998. Lipid domain structure of the plasma membrane revealed by patching of membrane components. J. Cell Biol. **141:**929–942.
18. **Hofman, E. G., et al.** 2008. EGF induces coalescence of different lipid rafts. J. Cell Sci. **121:**2519–2528.
19. **Kaleeba, J. A., and E. A. Berger.** 2006. Kaposi's sarcoma-associated herpesvirus fusion-entry receptor: cystine transporter xCT. Science **311:**1921–1924.
20. **Kowanetz, K., et al.** 2004. Suppressors of T-cell receptor signaling Sts-1 and Sts-2 bind to Cbl and inhibit endocytosis of receptor tyrosine kinases. J. Biol. Chem. **279:**32786–32795.
21. **Krishnan, H. H., et al.** 2004. Concurrent expression of latent and a limited number of lytic genes with immune modulation and antiapoptotic function by Kaposi's sarcoma-associated herpesvirus early during infection of primary endothelial and fibroblast cells and subsequent decline of lytic gene expression. J. Virol. **78:**3601–3620.
22. **Krishnan, H. H., N. Sharma-Walia, D. N. Streblow, P. P. Naranatt, and B. Chandran.** 2006. Focal adhesion kinase is critical for entry of Kaposi's sarcoma-associated herpesvirus into target cells. J. Virol. **80:**1167–1180.
23. **Le Blanc, I., et al.** 2005. Endosome-to-cytosol transport of viral nucleocapsids. Nat. Cell Biol. **7:**653–664.
24. **Levkowitz, G., et al.** 1998. c-Cbl/Sli-1 regulates endocytic sorting and ubiquitination of the epidermal growth factor receptor. Genes Dev. **12:**3663–3674.
25. **Li, M., et al.** 2003. Mono- versus polyubiquitination: differential control of p53 fate by Mdm2. Science **302:**1972–1975.
26. **Macdonald, J. L., and L. J. Pike.** 2005. A simplified method for the preparation of detergent-free lipid rafts. J. Lipid Res. **46:**1061–1067.
27. **Mark, L., W. H. Lee, O. B. Spiller, B. O. Villoutreix, and A. M. Blom.** 2006. The Kaposi's sarcoma-associated herpesvirus complement control protein (KCP) binds to heparin and cell surfaces via positively charged amino acids in CCP1-2. Mol. Immunol. **43:**1665–1675.
28. **Mineo, C., G. L. James, E. J. Smart, and R. G. Anderson.** 1996. Localization of epidermal growth factor-stimulated Ras/Raf-1 interaction to caveolae membrane. J. Biol. Chem. **271:**11930–11935.
29. **Naranatt, P. P., S. M. Akula, C. A. Zien, H. H. Krishnan, and B. Chandran.** 2003. Kaposi's sarcoma-associated herpesvirus induces the phosphatidylinositol 3-kinase-PKC-zeta-MEK-ERK signaling pathway in target cells early during infection: implications for infectivity. J. Virol. **77:**1524–1539.
30. **Nichols, B. J., et al.** 2001. Rapid cycling of lipid raft markers between the cell surface and Golgi complex. J. Cell Biol. **153:**529–541.
31. **Patel, K. P., C. B. Coyne, and J. M. Bergelson.** 2009. Dynamin- and lipid raft-dependent entry of decay-accelerating factor (DAF)-binding and non-DAF-binding coxsackieviruses into nonpolarized cells. J. Virol. **83:**11064–11077.
32. **Pietiainen, V., et al.** 2004. Echovirus 1 endocytosis into caveosomes requires lipid rafts, dynamin II, and signaling events. Mol. Biol. Cell **15:**4911–4925.
33. **Pike, L. J.** 2003. Lipid rafts: bringing order to chaos. J. Lipid Res. **44:**655–667.
34. **Pike, L. J., X. Han, and R. W. Gross.** 2005. Epidermal growth factor receptors are localized to lipid rafts that contain a balance of inner and outer leaflet lipids: a shotgun lipidomics study. J. Biol. Chem. **280:**26796–26804.
35. **Popik, W., T. M. Alce, and W. C. Au.** 2002. Human immunodeficiency virus type 1 uses lipid raft-colocalized CD4 and chemokine receptors for productive entry into CD4(+) T cells. J. Virol. **76:**4709–4722.
36. **Raghu, H., et al.** 2007. Lipid rafts of primary endothelial cells are essential for Kaposi's sarcoma-associated herpesvirus/human herpesvirus 8-induced phosphatidylinositol 3-kinase and RhoA-GTPases critical for microtubule dynamics and nuclear delivery of viral DNA but dispensable for binding and entry. J. Virol. **81:**7941–7959.
37. **Raghu, H., N. Sharma-Walia, M. V. Veettil, S. Sadagopan, and B. Chandran.** 2009. Kaposi's sarcoma-associated herpesvirus utilizes an actin polymerization-dependent macropinocytic pathway to enter human dermal microvascular endothelial and human umbilical vein endothelial cells. J. Virol. **83:**4895–4911.
38. **Sadagopan, S., et al.** 2009. Kaposi's sarcoma-associated herpesvirus upregulates angiogenin during infection of human dermal microvascular endothelial cells, which induces 45S rRNA synthesis, antiapoptosis, cell proliferation, migration, and angiogenesis. J. Virol. **83:**3342–3364.
39. **Sandvig, K., and B. van Deurs.** 2002. Transport of protein toxins into cells: pathways used by ricin, cholera toxin and Shiga toxin. FEBS Lett. **529:**49–53.
40. **Schmidt, M. H., and I. Dikic.** 2005. The Cbl interactome and its functions. Nat. Rev. Mol. Cell Biol. **6:**907–918.
41. **Sharma-Walia, N., et al.** 2010. Kaposi's sarcoma associated herpes virus (KSHV) induced COX-2: a key factor in latency, inflammation, angiogenesis, cell survival and invasion. PLoS Pathog. **6:**e1000777.
42. **Simons, K., and D. Toomre.** 2000. Lipid rafts and signal transduction. Nat. Rev. Mol. Cell Biol. **1:**31–39.
43. **Song, K. S., et al.** 1996. Co-purification and direct interaction of Ras with caveolin, an integral membrane protein of caveolae microdomains. Detergent-free purification of caveolae microdomains. J. Biol. Chem. **271:**9690–9697.
44. **Thien, C. B., and W. Y. Langdon.** 2001. Cbl: many adaptations to regulate protein tyrosine kinases. Nat. Rev. Mol. Cell Biol. **2:**294–307.
45. **Valiya Veettil, M., S. Sadagopan, N. Kerur, S. Chakraborty, and B. Chandran.** 2010. Interaction of c-Cbl with myosin IIA regulates Bleb associated macropinocytosis of Kaposi's sarcoma-associated herpesvirus. PLoS Pathog. **6:**e1001238.
46. **Varghese, B., et al.** 2008. Polyubiquitination of prolactin receptor stimulates its internalization, postinternalization sorting, and degradation via the lysosomal pathway. Mol. Cell. Biol. **28:**5275–5287.
47. **Veettil, M. V., et al.** 2008. Kaposi's sarcoma-associated herpesvirus forms a multimolecular complex of integrins (alphaVbeta5, alphaVbeta3, and alpha3beta1) and CD98-xCT during infection of human dermal microvascular endothelial cells, and CD98-xCT is essential for the postentry stage of infection. J. Virol. **82:**12126–12144.
48. **Veettil, M. V., et al.** 2006. RhoA-GTPase facilitates entry of Kaposi's sarcoma-associated herpesvirus into adherent target cells in a Src-dependent manner. J. Virol. **80:**11432–11446.
49. **Wang, F. Z., S. M. Akula, N. P. Pramod, L. Zeng, and B. Chandran.** 2001. Human herpesvirus 8 envelope glycoprotein K8.1A interaction with the target cells involves heparan sulfate. J. Virol. **75:**7517–7527.
50. **Wang, F. Z., S. M. Akula, N. Sharma-Walia, L. Zeng, and B. Chandran.**

2003. Human herpesvirus 8 envelope glycoprotein B mediates cell adhesion via its RGD sequence. J. Virol. **77:**3131–3147.

51. **Wang, X., D. Y. Huang, S. M. Huong, and E. S. Huang.** 2005. Integrin alphavbeta3 is a coreceptor for human cytomegalovirus. Nat. Med. **11:**515–521.
52. **Zhu, D., W. C. Xiong, and L. Mei.** 2006. Lipid rafts serve as a signaling platform for nicotinic acetylcholine receptor clustering. J. Neurosci. **26:**4841–4851.
53. **Zhu, F. X., X. Li, F. Zhou, S. J. Gao, and Y. Yuan.** 2006. Functional characterization of Kaposi's sarcoma-associated herpesvirus ORF45 by bacterial artificial chromosome-based mutagenesis. J. Virol. **80:**12187–12196.